The production and decay of sigma hyperons by kaons at rest

Muzahim Mohammed Abdullah

The Production and Decay of Sigma Hyperons by Kaons at Rest

A Thesis presented

by

MUZAHIM MOHAMMED ABDULLAH

for the

Degree of Master of Science

at the

University of Durham

September 1977

T O M Y P A R E N T S

ABSTRACT

A sample of 22354 $\bar{K}$-meson interactions at rest leading to the channels

$$\bar{K}P \longrightarrow \Sigma^{\pm}\pi^{\mp}$$

has been obtained from an exposure to the British National Hydrogen Bubble Chamber containing a track sensitive target. The data have been used to determine Γ, which is the ratio of the production of Σ^- hyperons to the production of Σ^{+-} hyperons. The quantity B, which is the branching fraction of Σ^{+-} hyperons into positive pions has been determined simultaneously.

The value of B ($=0.487\pm0.008$) is in close agreement with the known world value which gives confidence in the sample and in the method that have been used to determine B and Γ. The value of Γ ($=2.35\pm0.07$) resolve the existing discrepancy between the known measured values.

This thesis contains a description of the importance of Γ, an account of the experiment including a detailed consideration of how the ratios were determined.

CONTENTS

LIST OF FIGURES

LIST OF TABLES

CHAPTER ONE THE RATIO, Γ

1.1 Introduction

There have been several attempts to study $\bar{K}P$ interactions (ref.1,2,6) at low momenta within the momentum range (0-550)Mev/c. Because this momentum range limits the experimental technique almost entirely to the bubble chamber method, the statistical weights of the experiments, particularly the early ones, tend to be low. The reactions which occur chiefly are:

$$K P \longrightarrow \bar{K}P \quad (1)$$
$$\longrightarrow \bar{K}^{o} n \quad (2)$$
$$\longrightarrow \Sigma^{-}\pi^{+} \quad (3)$$
$$\longrightarrow \Sigma^{+}\pi^{-} \quad (4)$$
$$\longrightarrow \Sigma^{o}\pi^{o} \quad (5)$$
$$\longrightarrow \Lambda\pi^{o} \quad (6)$$

Although the $\bar{K}P$ reactions are dominated by three sets of two body final states $\bar{K}N$, $\Sigma\pi$ and $\Lambda\pi$, multipion production (e.g. $\Sigma\pi\pi$, $\Lambda\pi\pi$) is possible, but in the low momentum region it amounts to less than 1% of the total cross section. With charge independence the reactions above involve the two isopin states T = 0 and 1, whereas reaction 5 occurs in isopin T=0 and reaction 6 is isopin T = 1.

Models of the K-matrix type have been developed by Dalitz and Tuan (3) and others for the analysis of the low momentum data on the K-interaction Unfortunately the experimental data are insufficient to allow a determination of the K-matrix parameters. Instead an s-wave, constant-scattering length parameterisation has been used which involves 6 quantities only and which can be determined from the cross-section of the six reactions above. In this parameterisation of the KN reaction given by Dalitz and Tuan, the $\bar{K}P$ elastic and charge exchange cross-sections are expressed in terms of two complex constant scattering lengths, $A_o = a_o + ib_o$ and $A_1 = a_1 + i\, b_1$ for the isopin 0 and 1 channels respectively. Besides these four real parameters contained

in Ao and A_1, two more parameters are necessary to express the observed kaon cross sections. These parameters are chosen as a) the ratio (ϵ) of the $\Lambda\pi^0$ production rate to the total hyperon rate in the isopin 1 channel and, b) the phase angle between the isopin 0 and 1 amplitudes.

Then the kaon cross-sections are(reference 1)

$$\frac{d\sigma_{Kp}}{d\Omega} = \left| \frac{\csc^2\theta/2}{2Bk^2} \exp\left[\frac{2i}{kB}\ln\sin\theta/2\right] + C^2/2 \frac{A_o + A_1 - 2ik_oA_oA_1}{D} \right|^2 \qquad (7)$$

where θ is the scattering angle

$$\sigma_{K^0n} = \frac{\pi k_o C^2}{k^2} \left| \frac{A_1 - A_o}{D} \right|^2 \qquad (8)$$

$$\sigma_{\Sigma^+\pi^-} = \frac{1}{6}\sigma_o + \frac{1}{4}(1-\epsilon)\sigma_1 - \sqrt{\frac{1}{6}\sigma_o\sigma_1(1-\epsilon)}\cos\Phi \qquad (9)$$

$$\sigma_{\Sigma^-\pi^+} = \frac{1}{6}\sigma_o + \frac{1}{4}(1-\epsilon)\sigma_1 + \sqrt{\frac{1}{6}\sigma_o\sigma_1(1-\epsilon)}\cos\Phi \qquad (10)$$

$$\sigma_{\Sigma^0\pi^0} = \frac{1}{6}\sigma_o \qquad (11)$$

$$\sigma_{\Lambda\pi^0} = \frac{1}{2}\sigma_1\epsilon \qquad (12)$$

In the above,

$D = 1 - i\,(k_o + c^2k(1-i\lambda))\tfrac{1}{2}\,(A_o+A_1) - k_o(c^2k(1-i\lambda))\,A_oA_1$;

k_o = the wave number (centre-of-mass ystem) of the K^0n channel (taken as i/k_o / below K^0n threshold), k = the centre-of-mass wave number of K^-P channel, c^2 = the coulomb penetration factor = $(2\pi/kB)\,(1-\exp(-2\pi/kB))^{-1}$, B is the Bohr absorption cross-section in the T= o, T = 1 channels.

In these expressions the ratio (ϵ) is given by

$$\epsilon = \frac{\sigma_\Lambda}{\sigma_1} = \frac{q_\Lambda |N_1|^2}{q_\Sigma |M_1|^2 + q_\Lambda |N_1|^2} \qquad (13)$$

and the phase angle is defined by

$$\Phi = \mathrm{Arg}\left[\frac{M_o(1-ik_oA_1)}{N_1(1-ik_oA_o)}\right] = \Phi_{th} + \mathrm{Arg}\left(\frac{1-ik_oA_1}{1-ik_oA_o}\right) \qquad (14)$$

where $\Phi_{th} = \text{Arg}\left(\frac{Mo}{M_1}\right)$ is the phase difference at $\bar{K}N$ threshold and Mo, M_1 and N_1 are the reaction amplitudes in T = 0 and 1 states for $\Sigma(Mo, M_1)$ and $\Lambda(N_1)$ respectively.

Dalitz and Tuan found with the then existing data that two solutions fitted the data above threshold. Subsequently with the data of Kim(1) one solution was eliminated. For the acceptable solution Kim's parameters are

$a_o = -1.674 \pm 0.038$ fm, $\quad b_o = 0.729 \pm 0.04$fm

$a_1 = -0.070 \pm 0.058$ fm, $\quad b_1 = 0.688 \pm 0.33$fm

$E = 0.318 \pm 0.021 \quad \Phi_{th} = -53.8^{o}$

The main result of the scattering length fits is the prediction from the negative value of a_o of a $\bar{K}p$ bound state which is identified as the $\Lambda(1405)$ resonance. Its presence must be taken into account in the determination of the ΛKN and ΣKN coupling constants g^2_Λ and g^2_Σ from forward KN dispersion relations (reference 4).

To study the region below threshold (assuming that extrapolation of the amplitudes from the physical region to unphysical region is possible) the data for K^- absorption at rest can be considered (that is when, a kaon in a mesic atom undergoes capture by virtual mucleons bound in the nucleus).

The Γ -ratios, (Γ = Σ^- production/ Σ^+ production) have been observed for K^- capture in some heavy nuclei, (reference 4) and are displayed as $1/\Gamma$ in Figure 1 . The ratio has been measured in deuterium ($\Gamma = 1.14 \pm 0.13$), helium ($\Gamma = 0.29 \pm 0.03$), and in nuclear emulsion using heavy nuclei ($\Gamma = 0.84 \pm 0.09$) and light nuclei ($\Gamma = 0.58 \pm 0.06$). They are compared with the value for hydrogen in Figure 1 . Also shown in the figure are the expected values of Γ assuming various scattering length models. The values of centre of mass energy below threshold are uncertain. They are estimated from the average energy that would be needed to extract the proton (on

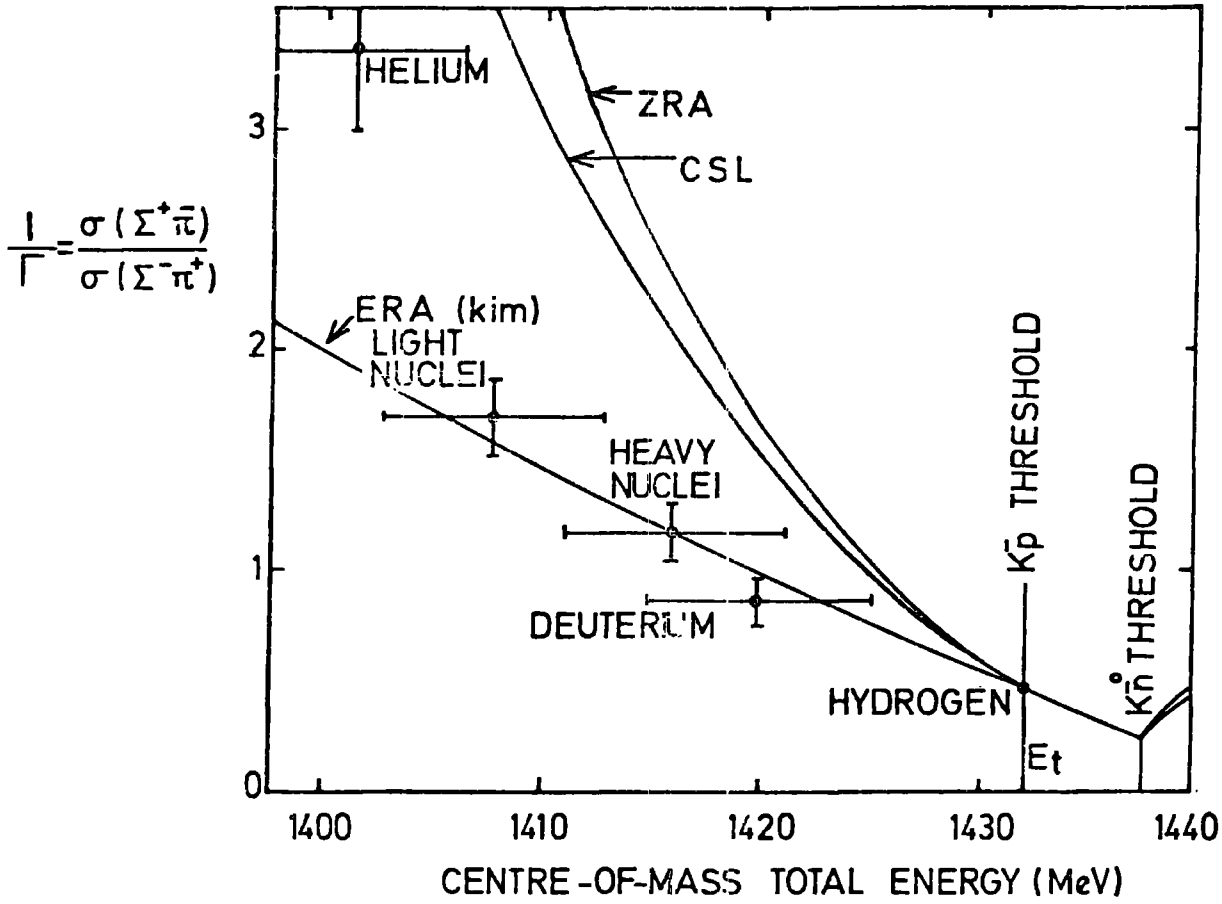

FIG. 1. A COMPARISON OF THE RATIO $\sigma(\Sigma^+\pi^-)/\sigma(\Sigma^-\pi^+)$ CALCULATED BY EXTRAPOLATING THE K^-p SOLUTIONS BELOW THRESHOLD WITH THE VALUES OBTAINED FROM THE K^- NUCLEAR CAPTURE DATA. THE CURVES ARE EXPECTED VALUES FOR $1/\Gamma$ FOR THE EFFECTIVE RANGE APPROXIMATION (ERA), ZERO RANGE APPROXIMATION (ZRA) AND CONSTANT SCATTERING LENGTHS (CSL).

which the capture occurs) from the nucleus. Many factors have been neglected such as secondary interactions in the same nucleus (e.g. $\Sigma P \longrightarrow \Lambda n$ OR $\Sigma^{o} n$, $\Sigma^{+} n \longrightarrow \Lambda P$ OR $\Sigma^{o} P$) multiple scattering, and the possibility of real Y* production (reference 3).

The ratio is of prime importance in the establishment of the $\bar{K}N$ reaction matrix since it determines the relative phase between the T=0 and T=1 amplitudes in the channel. In fact if the behaviour of this ratio below the $\bar{K}P$ threshold could be reliably set free from the effect introduced by the presence of other various nuclear properties, a study of ($\Sigma^{\pm} \pi^{\mp}$) production in nuclei could provide results of great interest in the region just below $\bar{K}p$ threshold ($\Lambda(1405)$) and would differentiate between solutions of the K-matrix which only diverge appreciably below the $\bar{K}P$ threshold.

The value of Γ in hydrogen at threshold has been determined by Kim(1) using a hydrogen bubble chamber. The value was found to be (2.06 ± 0.06). It has also been determined by Tovee (5) using the hydrogen in nuclear emulsion where the value is (2.34 ± 0.08). (As a general observation it is interesting to note that there are only two experimental studies with relatively high statistics of the $\bar{K}p$ interation at low momenta ($p_{\bar{K}}$ 300Mev/c) (reference 6), but only one, that of Kim, involves a study of all final states.)

The two results above differ by about three standard deviations. Because of this experimental situation and because of the importance of Γ to extrapolation into the non-physical region, a further determination of this ratio should be made. The method of analysis adopted by Kim in determining the ratio Γ for $\bar{K}$-meson captures at rest on proton is not clearly stated in his thesis. He only remarks that his sample comprised (4994) Σ^{-} and (2429) Σ^{+}. However if it is to be assumed that he used the same range and angular selections of these data as he himself used when determining the in-flight $\bar{K}P \longrightarrow \Sigma^{\pm} \pi^{\mp}$ cross-sections, (or those explicitly stated by Chang (reference 7) when determining the $\Sigma^{\pm}$ hyperon lifetimes using

the same film), then the remark of Eisele (reference 8) is appropriate. This concerns the biases, arising from uncertainties in measurement errors when they are comparable with the length of the tracks measured and which are known to occur for lifetime measurements. Since the number of events excluded by a given short range cut ($\sim$1mm) on the track of a Σ hyperon is significant and moreover strongly dependent on the sign of its charge through the lifetime τ. ($\tau_{\Sigma^-} \sim 2\tau_{\Sigma^+}$) then uncertainty in the application of this length criterion will lead to larger effects with Σ^+ than with Σ^- hyperons. This is well illustrated by the results of a calculation given in table 1 . Those sigma hyperons produced in $\bar{K}p$ interations at rest are considered in a calculation where measurement errors on track length are taken into account via a gaussian distribution. The loss of events, when a minimum track length is required, is estimated and shown in table 1 . As can be seen the losses are substantial and larger for Σ^+ than for Σ^- The correction factor by which the observed ratio Γ should be multiplied is also shown. For errors in the range of 0.0 to 1.5 mm the correction factors themselves are uncertain from about 4% to 20%. Obviously without an exact knowledge of the size of the measuring accuracy it will not be possible to determine the ratio of Σ^-/Σ^+ to any great precision by using only those events in which the lengths of the sigma tracks are greater than some minimum value. From the results presented in table 1 it is evident that probably an unattainably precise knowledge of the measurement error is essential to make a sensible determination of Γ accurate to within a few persent by this method (lifetime method). In addition the measurement error in the $\Sigma^\pm$ production and decay points causes a considerable spreading out of the observed time distribution. This is illustrated in Figure 2 where the apparent life time of $\Sigma^\mp$ is shown as function of measuring error in mms. In the range of typical measuring errors (0.5-1mm) the apparent lifteime of the Σ^+ is increased by 4% and that of the Σ^- by 3%.

TABLE. 1.

CUT OFF (mm)	Σ^- %	Σ^+ %	Σ^-/Σ^+ CORRECTION	Σ^- %	Σ^+ %	Σ^-/Σ^+ CORRECTION	Σ^- %	Σ^+ %	Σ^-/Σ^+ CORRECTION
	ZERO ERROR			ERROR 0.5 mm			ERROR 1.0 mm		
0.5	7.2	12.0	0.948	5.5	9.0	0.958	4.3	7.0	0.971
1.0	13.8	24.0	0.882	11.2	19.5	0.907	9.5	15.0	0.939
1.5	20.3	35.5	0.809	17.4	27.5	0.878	14.3	23.0	0.898
2.0	26.4	47.5	0.713	22.8	39.0	0.790	19.9	31.5	0.855

PERCENTAGE LOSSES AND CORRECTION FACTORS OF $\Sigma^{\pm}$ HYPERONS WHEN A MINIMUM OBSERVABLE LENGTH IS REQUIRED, (CUT OFF LENGTH), IN THE PRESCENCE OF MEASURING ERRORS OF 0, 0.5 AND 1.0 mm.

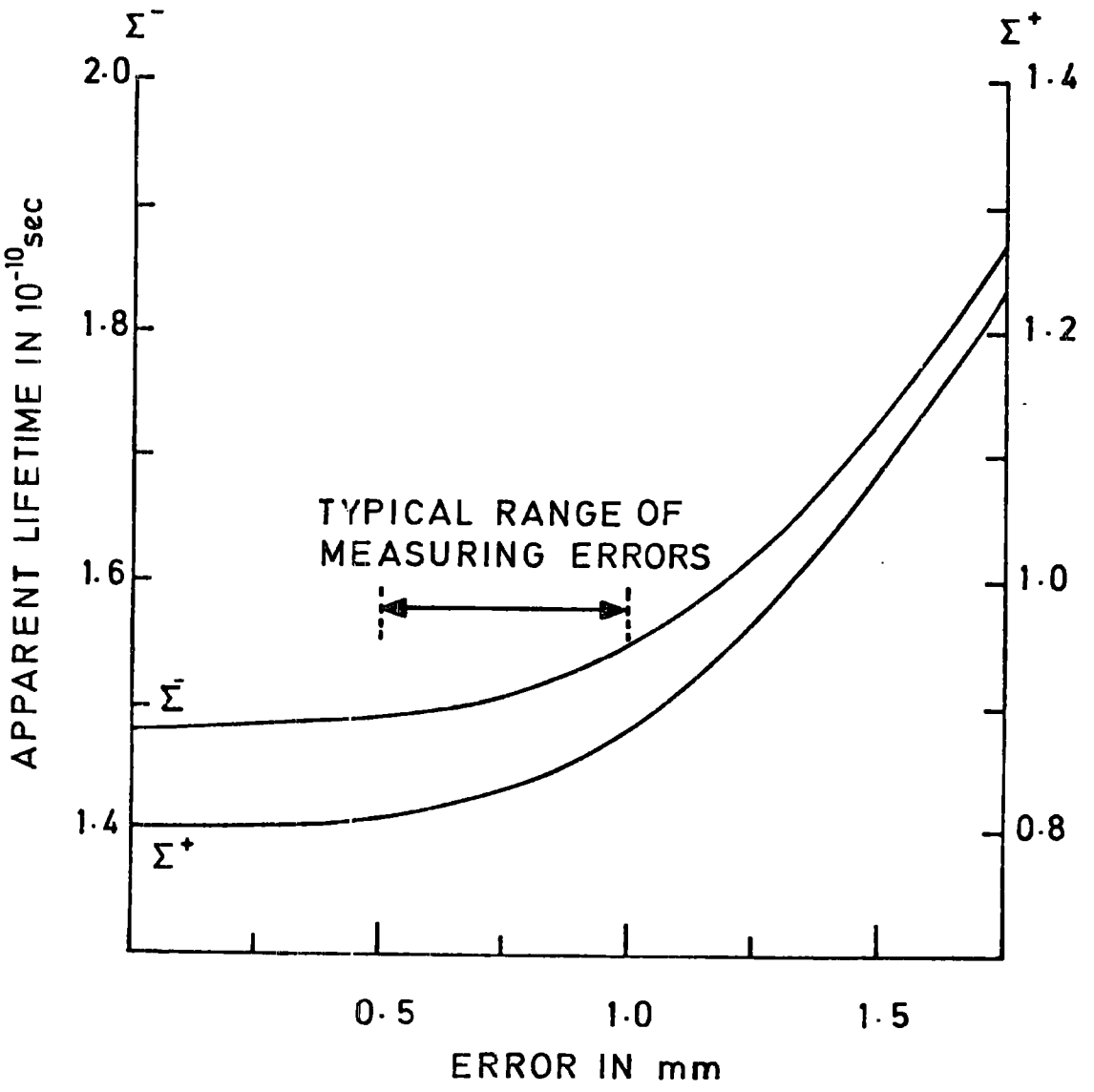

FIG. 2 THE APPARENT LIEFTIME AS A FUNCTION OF MEASURING ERROR

1.2 Methods of Determining Γ

Two methods of determining Γ will be employed. In the first of these the objection, discussed above to the use of events where the Σ^--hyperons are larger than some minimum length, is overcome by using all Σ^--hyperon events above and below the minimum length. In the second method, essentially a minimum length is determined which corresponds to an effective zero measuring error.

a) Method one

This method of analysis avoids any range and angular selections and consequently biases associated with them. The major difficulty is that at low energy, Σ_S have short lengths before decay and so in some $\Sigma^{\pm}\pi^{\mp}$ events the $\Sigma^{\pm}$ is not visible and only the production and decay pions are seen ($\pi^+\pi^-$ events). The philosophy of this method is to avoid attempting to separate the $\pi^+\pi^-$ events, by scanning and measuring, into Σ^- and Σ^+ categories. Instead the number of Σ^+ decaying into pions is determined from the number decaying into protons through the known branching ratio

$$B = \frac{\Sigma^+ \longrightarrow \pi^+ n}{\Sigma^+ \longrightarrow p\pi^o + \Sigma^+ \longrightarrow n\pi^+}, \quad (B = 0.4835 \pm 0.007) \text{ (reference 9).}$$

It is necessary to define categories of events as follows:

$N_{\Sigma^-_{\pi}}$ - expected number of $\Sigma^- \longrightarrow \pi^- n$ decay.

$N_{\Sigma^-_{\pi}(obs)}$ - observed number of such decays where the Σ^- is seen.

$N_{\Sigma^-_{\sigma}(obs)}$ - observed number of Σ^- absorption.

$N_{\pi^+\pi^-(obs)}$ - observed unresolved $\pi^{\pm}\Sigma^{\mp}(\longrightarrow \pi^{\mp} + n)$ events where the $\Sigma^{\pm}$ cannot be seen.

$N_{\Sigma^+_{\pi}}$ - expected number $\Sigma^+ \longrightarrow \pi^+ n$ decays.

$N_{\Sigma^+_{\pi}(obs)}$ - observed number of such decays where the Σ^+ is seen.

$N_{\Sigma^+_{p}(obs)}$ - observed number of $\Sigma^+ \longrightarrow p\pi^o$ decays.

N_{π^-p} - observed number of Σ^+ decay to $p\pi^o$ where the Σ^+ is not seen.

From these categories the total numbers N^+, N^- of Σ^+ & Σ^- events can be calculated from which $\Gamma = N^-/N^+$

Firstly,

$$N^+ = N_{\Sigma^+ \longrightarrow p}(\text{obs}) + N_{\pi^- p} + N_{\Sigma^+ \longrightarrow \pi\pi}(\text{obs}) + f_+ (\pi^+\pi^-) \quad \ldots\ldots(15)$$

where f_+ is an unknown fraction of the $\pi^+\pi^-$ events. However, from the ratio, B, the last terms of the right hand side of equation (15) can be replaced and

$$N^+ = \frac{N_{\Sigma_p^+}(\text{obs}) + N_{\pi^- p}}{1 - B} \qquad (16)$$

Secondly,

$$N^- = N_{\Sigma_\sigma^-}(\text{obs}) + N_{\Sigma_{\pi\pi}^-} \qquad (17)$$

$$= N_{\Sigma_\sigma^-}(\text{obs}) + N_{\Sigma_{\pi\pi}^-}(\text{obs}) + f_-(\pi^+\pi^-) \qquad (18)$$

where f_- is an unknown fraction. It can be replaced and

$$N^- = N_{\Sigma_\sigma^-}(\text{obs}) + N_{\Sigma_{\pi\pi}^-}(\text{obs}) + N_{\pi^+\pi^-}(\text{obs}) - f_+ (\pi^+\pi^-) \qquad (19)$$

$$= N_{\Sigma_\sigma^-}(\text{obs}) + N_{\Sigma_{\pi\pi}^-}(\text{obs}) + N_{\pi^+\pi^-}(\text{obs}) - (N_{\Sigma_{\pi\pi}^+} - N_{\Sigma_{\pi\pi}^+}(\text{obs})) \qquad (20)$$

$$= N_{\Sigma_\sigma^-}(\text{obs}) + N_{\Sigma_{\pi\pi}^-}(\text{obs}) + N_{\Sigma_{\pi\pi}^+}(\text{obs}) + N_{\pi^+\pi^-}(\text{obs}) - N_{\Sigma_{\pi\pi}^+} \qquad (21)$$

replacing $N_{\Sigma_{\pi\pi}^+}$ as before

$$N^- = N_{\Sigma_\sigma^-}(\text{obs}) + N_{\Sigma_{\pi\pi}^-}(\text{obs}) + N_{\Sigma_{\pi\pi}^+}(\text{obs}) + N_{\pi^+\pi^-}(\text{obs}) - \frac{B}{1-B}\left[N_{\Sigma^+}(\text{obs}) + N_{\pi^- p}\right] \qquad (22)$$

By this approach it is clear that accurate separation of $\Sigma \longrightarrow \pi\pi$ decays into Σ^- and Σ^+ is not necessary as long as the total number is counted. All that is required is an accurate estimation of the total number of $\Sigma^+ \longrightarrow p$ decays in the two cases where a) the Σ^+ is clearly visible and b) where the Σ^+ is not clearly visible but is readily identified by the proton involved in the decay. At the energies involved in this experiment there is no possibility whatsoever (except in the case of very steep tracks) where the π^+ and proton from Σ^+ decay can be confused. Hence the

accuracy of the determination of Γ is based on determining a clearly recognisable decay. Except in a small number of cases no measurements need to be involved since all judgements can be made at the scanning table. Obviously the emphasis is on very high scanning efficiency and interpretation of events. Consequently this kind of scanning has to be done by experienced workers. In this experiment it was carried out by trained physicists.

b) Method two

In the previous method no attempt was made to divide the $\pi^+\pi^-$ events into those originating from Σ^+ & Σ^- respectively. If it assumed that the limit of resoltuion for detecting the decay of a Σ^-_π is exactly the same as that for Σ^+_π then it is possible to divide the total number of $\pi^+\pi^-$ events into their charged Σ origins provided the limit of resolution can be determined. Suppose that the effective length that a hyperon must have before its charge can be recognised (by its decay secondary) is r, than the Γ ratio can be calculated as follows:

The number of Σ^- seen to decay or be absorbed is

$$(N_{\Sigma^-_\pi}(obs) + N_{\Sigma^-_\sigma}) = N_{\Sigma^-}\left(\exp\frac{-t_-(r)}{\tau_-}\right) \tag{23}$$

and the corresponding number of Σ^+_π decays is

$$N_{\Sigma^+_\pi}(obs) = N_{\Sigma^+_\pi}\left(\exp\frac{-t_+(r)}{\tau_+}\right) \tag{24}$$

where τ_-, τ_+ are the respective mean lives, t_- and t_+ are the respective times to travel distance r ($t_- \sim 1.055\ t_+$). Assuming, as in method (1), that the number of Σ^+ decays to proton is well determined and is given by $N_{\Sigma^+_p}$ then

$$\Gamma = \frac{N_{\Sigma^-_\pi}}{N_{\Sigma^+_\pi} + N_{\Sigma^+_p}} = \frac{(N_{\Sigma^-_\pi}(obs) + N_{\Sigma^-_\sigma})\, e^{t_-(r)/\tau_-}}{N_{\Sigma^+_\pi}(obs)\, e^{t_+(r)/\tau_+} + N_{\Sigma^+_p}} \tag{25}$$

The effective length, r, is determined from the number of observed events as follows.

$$N_{\pi^+\pi^-} = N_{\Sigma^-}\left(1-\exp\frac{-t_-(r)}{\tau_-}\right)+N_{\Sigma^+_{\pi}}\left(1-\exp\frac{-t_+(r)}{\tau_+}\right) \quad (26)$$

$$=\left(N_{\Sigma^-_{\pi}}(obs)+N_{\Sigma^-_{\sigma}}\right)\left(\exp\frac{t_-(r)}{\tau_-}-1\right)+N_{\Sigma^+_{\pi}}(obs)\left(\exp\frac{t_+(r)}{\tau_+}-1\right) \quad (27)$$

In this expression only r is unknown and hence it can be determined from the observed numbers of $\pi^+\pi^-$, Σ^-_{π}, Σ^-_{σ} and Σ^+_{π} events. Obviously, by substituting r back into the two right hand terms of equation (26), the numbers of $\pi^+\pi^-$, events are divided into those originating from Σ^- and Σ^+ respectively.

With this value of r substitution into equation (25) will yield the new estimate of Γ.

Furthermore, with the $\pi^+\pi^-$ events effectively separated it is possible to determine the branching ratio of the Σ^+ into pions and protons where

$$B=\frac{N_{\Sigma^+_{\pi}}(obs)+f_+N_{\pi^+\pi^-}}{N_{\Sigma^+_{\pi}}(obs)+f_+N_{\pi^+\pi^-}+N_{\Sigma^+_p}}=\frac{N_{\Sigma^+_{\pi}}(obs)e^{t_+(r)/\tau_+}}{N_{\Sigma^+_{\pi}}(obs)e^{t_+(r)/\tau_+}+N_{\Sigma^+_p}} \quad (28)$$

Hence the attraction of this second method is that it yields a new estimate of Γ and also a new estimate of B.

1.3 Summary

An account has been given of the relevance of the determination of the ratio.

$$\Gamma = \Sigma^-/\Sigma^+$$

to the low momentum interactions of kaons. The experimental discrepancy has been presented and two methods for further determination have been discussed in outline.

In the further parts of this thesis an account is given of the experimental application of those two methods. Firstly however the track sensitive target chamber that has been used is described together with an account of

the experimental runs and exposures. This is followed by a description of the scanning and measuring that was made and terminates with a discussion of the quality of the data. Finally, there is a discussion of the precision of the two methods of analysis leading to the final determination of Γ and the branching ratio B. In conclusion there is a short discussion and comparison of Γ with other experimental results and an indication is given of further work in this field.

CHAPTER TWO THE CHAMBER AND EXPOSURE

2.1 Introduction

The work described in this thesis is part of a general experiment on the interaction of low momentum kaons. In Chapter 1 the main reactions were described (equation 1 to 6). In particular reactions 5 and 6 involved the production of π^0 mesons and were given by

$$K^- P \longrightarrow \Sigma^0 \pi^0 \qquad (5)$$

$$K^- P \longrightarrow \Lambda^0 \pi^0 \qquad (6)$$

In reaction (5) the Σ^0 decays very rapidly ($\tau \sim 10^{-16}$ sec) into $\Lambda\gamma$. Consequently as seen in the normal hydrogen filled chamber these two reactions appear to be identical. What is seen in each case is a terminating kaon track with close by, a Λ -hyperon pointing to the track ending. Moreover, in measurement these reactions are very similar and there is a high degree of ambiguity between the interpretation of events consisting only of a kaon track with a pointing Λ .

To avoid this ambiguity (and hence being able to analyse pure T=0 and pure T=1 reactions) an attempt was made in this overall experiment to detect the γ rays associated with these reactions. If γ -detection is very efficient then the clear signatures of reaction 5 (3γ-rays) and reaction 6 (2γ-rays) lead to the resolution of the ambiguity.

In the conventional hydrogen filled chamber the radiation length χ, is about 10m, which leads to γ materialisation in a few percentage of cases only ($< 5\%$). In a heavy liquid filled chamber the radiation length, with a neon filling, for example, becomes about 25cm which leads to an increase in materialisation probability by a factor of about 40. Unfortunately the reduced radiation length also implies large coulomb scattering and

consequently measuring precision is lost.

In the present experiment an attempt was made to combine the advantage of light and heavy liquids by building a composite system of a hydrogen filled chamber inside a neon filled chamber (reference 10). The hydrogen is to be used for measurment of primary interaction vertices and secondary decay vertices and the neon is to be used to increase the probability of γ - materialisation.

Although this feature (γ - materialisation) is of no importance in the physics involved in determining the ratio $(\frac{\Sigma^-\text{production}}{\Sigma^+\text{production}})$ it does have experimental consequences by the limitations on track length which are set by the small volume of hydrogen. In the following sections the composite chamber will be described and special attention will be drawn to the advantages and disadvantages that it imposes on the experiment as a whole.

2.2. Description of the British National Hydrogen bubble chamber with Track Sensitive Target

The chamber figure 3 vessel is bounded by two-parallel windows of which the clear aperture is rectangular with semi-circular ends and having dimension 150cm by 50cm. The windows are 15.5cm thick and they are spaced 45 cm apart between the inner faces. Thus the effective volume of the chamber is about 300 litres (reference11). The chamber is photographed in dark field by an array of three cameras with parallel axes, perpendicular to the camera side main window. The cameras are placed 1.4m away from the chamber.

A reference system in the chamber is provided by set of crosses ruled on the inner surface of the main windows and on the outer surface of the camera side window.

Brief description of operation.

The chamber is run in a magnetic field of 12.3k gauss. Under normal conditions the conventional chamber is filled with hydrogen, made liquid by temperature (27 K) and pressure (8 Atmospheres). On

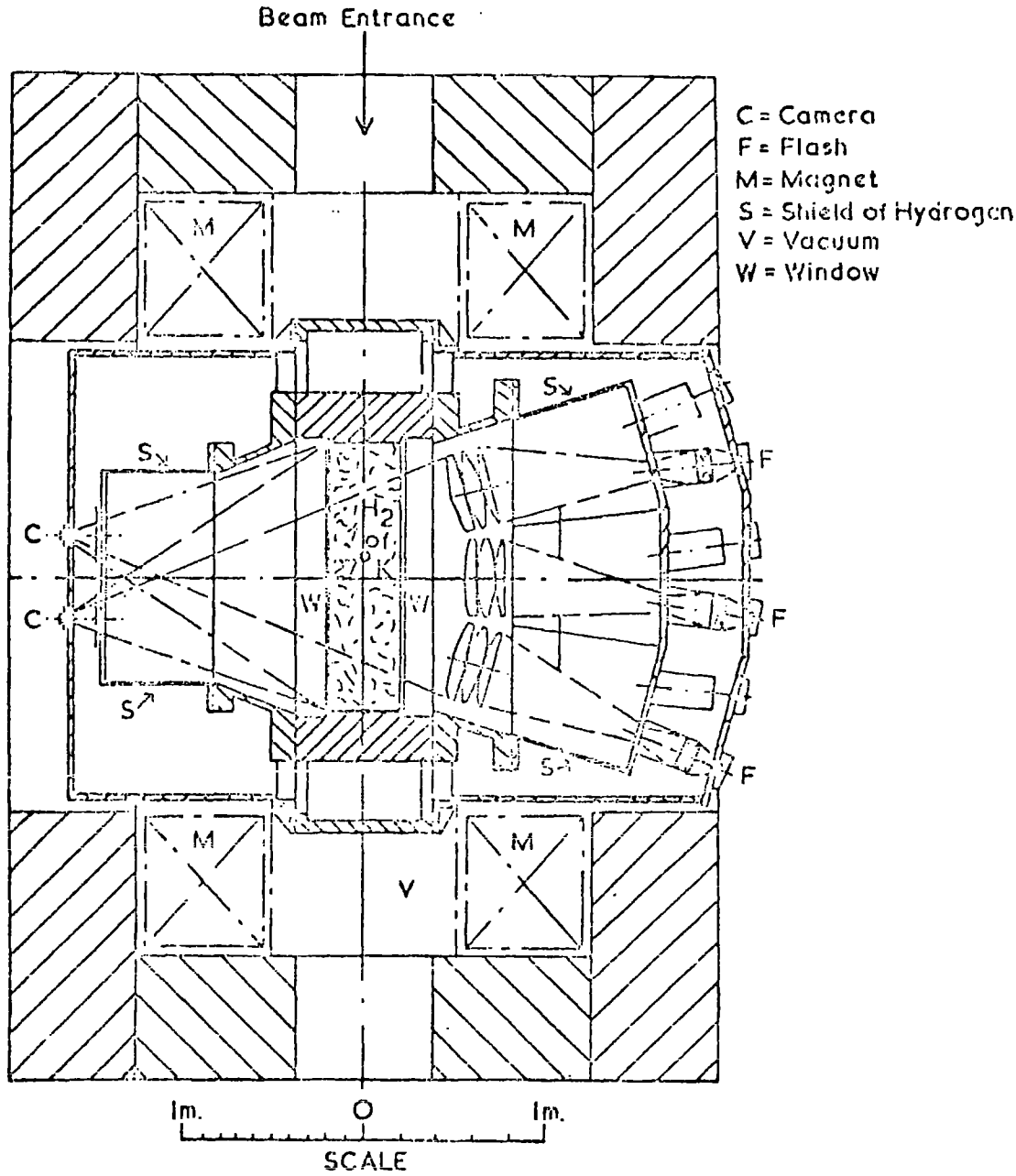

FIG. 3. PLAN VIEW OF B.N.H.B.C. SHOWING OPTICAL SYSTEM AND MAGNET

release of the pressure to about 4 Atmospheres the liquid hydrogen is now at a temperature above its boiling point. It can remain superheated for a few m secs before spontaneous boiling will occur. During this few milli secs the beam of particles have to pass through the chamber, cause bubbles to form at centres of ionisation, be photographed and the pressure restored to make the liquid stable again.

However the chamber is used, in the composite system, under slightly different conditions. The chamber has been modified to enable it to be used to with a target of liquid hydrogen surrounded by a neon-hydrogen mixture figure 4 . The two liquids which can be made superheated and hence made sensitive at a temperature of 29 K are separated by plexiglass windows which are the walls of the target. When the pressure of the outer part of the chamber is reduced the flexing of the plexiglass walls tramsits the necessary volume/pressure change to the hydrogen which also becomes sensitive. The plexiglass windows on either side of the central plane of the chamber define the depth of the T.S.T. as 7.85cm. The windows are 1.0cm thick. Fiducial marks are engraved on the outer surface of the T.S.T. walls. Two track sensitive targets have been successfully operated in the 1.5m cryogenic bubble chamber at the R.H.E.L. The first target was metal framed, whereas the second was made completely out of plexiglass.

a) Metal framed target:

The target (reference 12) consists of a strong stainless steel frame which is rigidly mounted in the chamber body.

The plexiglass windows are sealed to the frame with a gasket of indium wires, by inflating flexible steel tubes figure 5 . The interal dimensions are 135. x 33.5 x 7.8 cm^3 and the external are 147 x 44.7 x 9.8cm^3 .

This target reduces the gamma detection efficiency since the metal frame limits the useful visible region of the chamber.

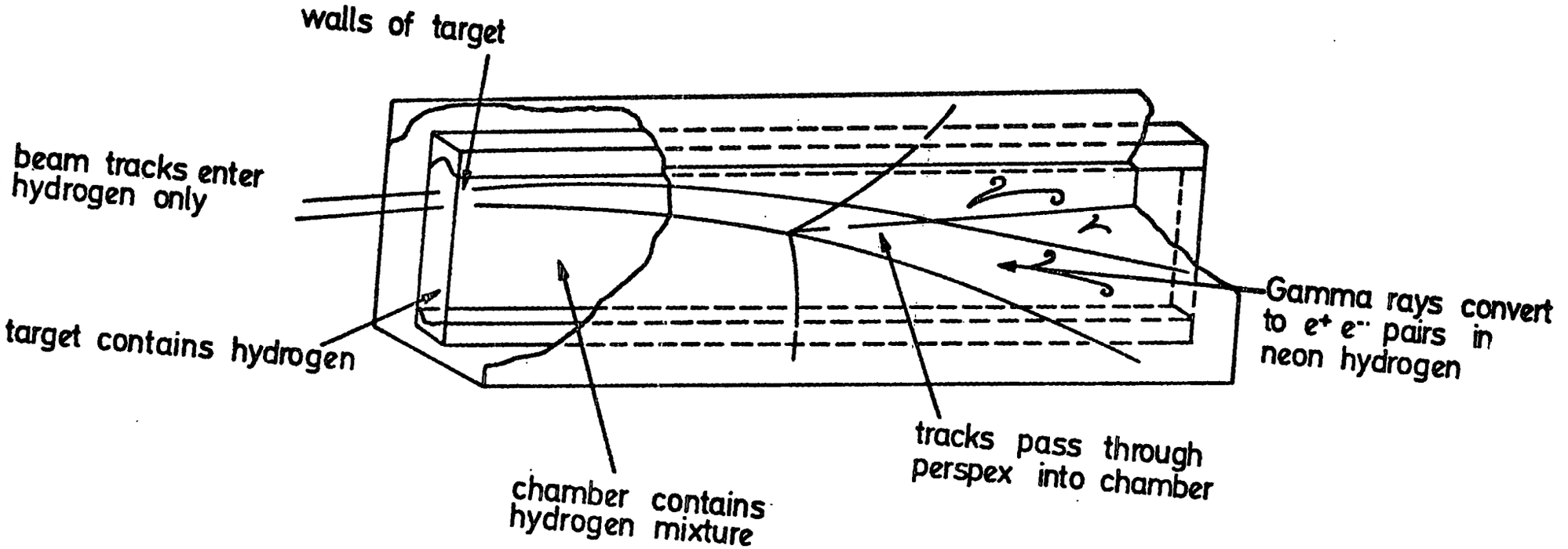

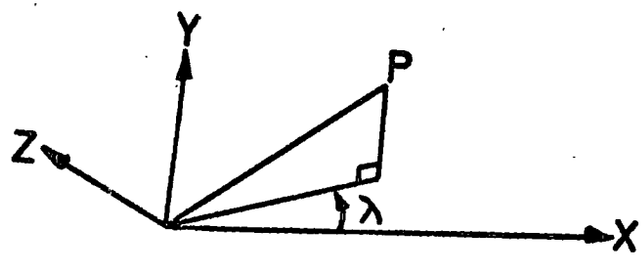

Co-ordinate system, origin at centre of chamber.

FIG. 4 SCHEMATIC DIAGRAM OF THE TRACK SENSITIVE TARGET INSIDE THE BUBBLE CHAMBER.

Fig.5 : The Composite target section. The beam enters directly into the hydrogen. The magnetic field produces a curvature in the plane of the target.

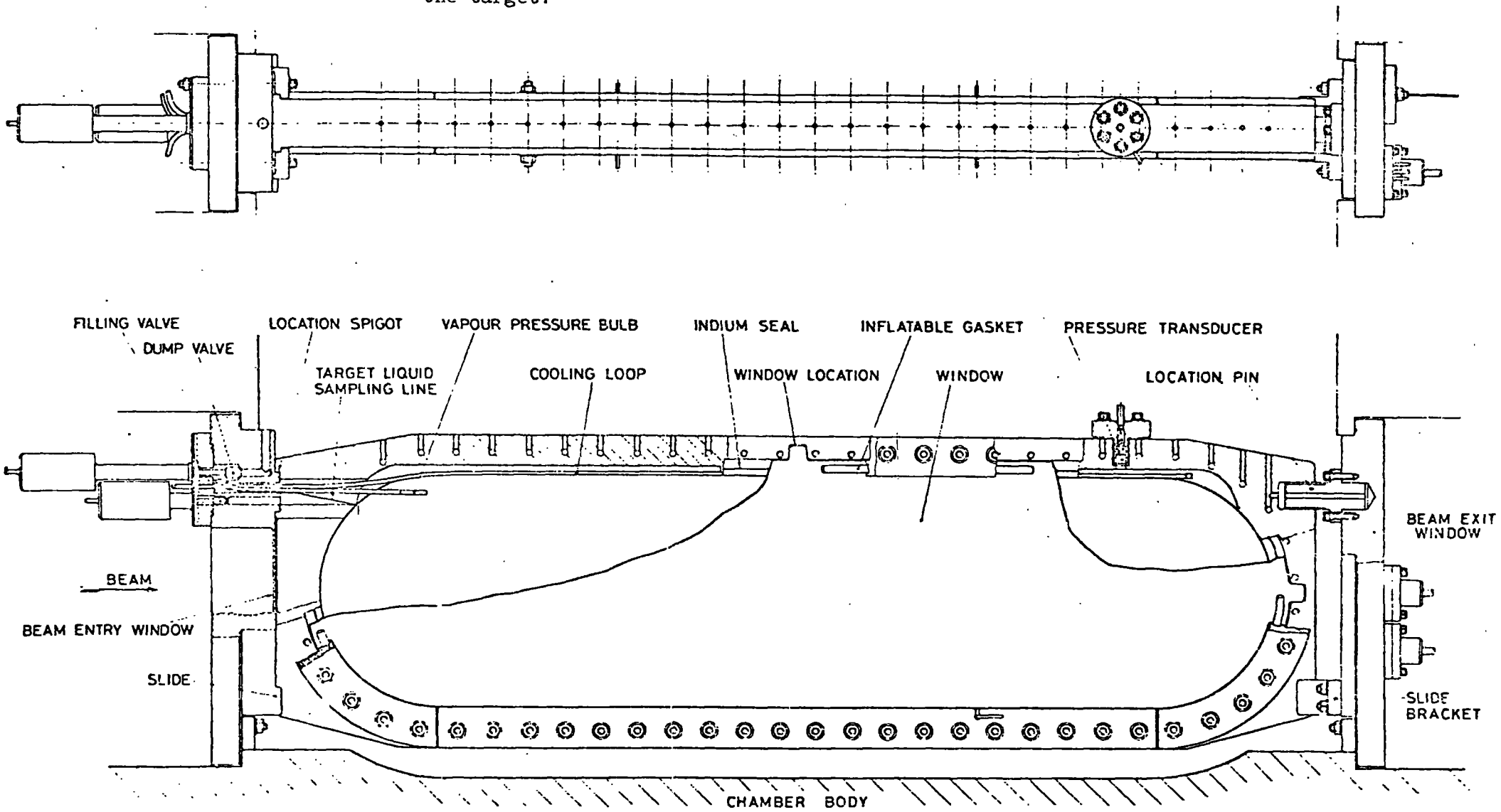

TRACK SENSITIVE TARGET FOR 1·5 METRE CHAMBER FIG.5

b) Plexiglass target (plastic framed target):

Since the composite target limited gamma detection, because of obscuration by the metal frame, it was decided to build an all plexiglass T.S.T. The essential simplicity of all plexiglass system is clear. The plexiglass is transparent to both charged particles, gamma rays and visible light and so the gamma efficiency is significantly increased. Whereas the metal framed target was mounted parallel to the windows of the outer chamber, the plexiglass T.S.T. was mounted at an angle to maximise the potential path length of primary kaons in the T.S.T.

c) Neon-Hydrogen mixture

Experimentally it is found that neon cannot be made to work as a bubble chamber liquid at a temperature close to the normal operation temperature of hydrogen as a bubble chamber liquid unless the neon is diluted with hydrogen. The richest mixture of neon-hydrogen that has been used is about 80% by number density. In the present experiment the number density varies from, initially about 70% to finally about 80%. In this range of mixture the radiation length in Ne/H2 is about 45cm long compared to the radiation length in hydrogen of 10m. This radiation length is smaller by a factor of about 20. This implies that the conversion probability for γ rays is increased by a factor of 20. Although this factor of 20 appears to be a very large increase it should be noted that this gives a conversion probability of about 30% for a single γ ray in the composite system described. Unfortunately, in this experiment (as distinct from the first experiment with T.S.T. chamber with 4Gev pions), the γ energies are quite low and in many cases the large energy loss and coulomb scattering of the electron in the γ conversion make it impossible to measure the γ energy. This reduces the effective conversion probability to about 15%. Consequently the improvement by factor of 20 is reduced to a factor of 10.

d) T.S.T. Advantages and Disadvantages:

Several advantages are to be gained from using the T.S.T. The main advantage is the gain of γ conversions but at the same time, precision of working in hydrogen is maintained, that is the target in unambigously a proton and measuring precision is high. Gamma rays from $\pi^0, \Sigma^0 \ldots$ etc. decay emerge through the perspex walls of the T.S.T. into the neon hydrogen mixture where they may be converted into electron-positron pairs and point to the production vertex. In practice there is no difficulty in associating gammas with the correct origin, although the electron and positron tracks have the characteristic heavy liquid features of large multiple scattering and bremsstrahlung. The efficiency for multi-gamma detection depends critically on the ratio of the conversion length (9/7x radiation length) for gamma to the dimension of the bubble chamber (reference 12).

The different track qualities in the two media are clear. The bubble size in the hydrogen turns out to be smaller ($\sim 200\mu$) than in a conventional chamber and this leads to increased measuring precision and improved resolution in the neighbourhood of vertices (~ 0.5mm). This is very important in the determination of the Σ^-/Σ^+ ratio at rest, where the small bubble size enables Σ^- & Σ^+ to be recognised down to smaller lengths than is usual in a hydrogen chamber. There is a further gain in precision for low momentum tracks which stop in neon. For these, range rather than curvature is measured leading to a considerable increase in precision. A general visual advantage is gained at scanning time and that is the steepness of tracks can be judged quite accurately by the length of the blank separation in plexiglass of the track hydrogen and its continuation in neon.

The main disadvantage of the T.S.T. system is the small depth of the chamber (7.8cm). The low momentum kaon beams have been produced by passing higher momentum beams through a degrader of about 30 cm Aluminium. The emergent kaons are dispersed in both the horizontal and vertical directions and consequently the potential path length is quite low at 49cm. instead of 150 cm. At low momenta the secondary particles tend towards isotropy and the shallow depth immediately restricts the potential lengths.

In this particular experiment where 0 Λ (that is a zero pronged primary vertex with an associated Λ) events form an important topological group for the inflight interaction, about one half of the 0 prong events that are scanned are in fact primary interactions in the perspex.

The chamber depth is important in the determination of the Γ ratio at rest. In a conventional chamber where there is little depth restriction Σ^{+} decay and Σ^{-} absorption are seen in their entirety (i.e.both primary and secondary vertices are seen). Here 1% of the secondary vertices occur in the T.S.T. walls because of narrowness of the chamber. To restrict events only to the central part of the chamber so that all events are complete would reduce the effective chamber depth by 25% which implies that 25% of the scanning in effect is made useless. Consequently, these incomplete events have to be used.

Normally at low mementa, Λ hyperons decay within a few cm of the vertex. Again with a shallow T.S.T. about 30% decay in the neon where curvature measurements are poor (because of coulomb scattering).

2.3 The exposure

The exposure took place in 1973 using a negative kaon beam transported at 600 meV/c directed into the hydrogen bubble chamber and degraded to lower momenta by an aluminium block mounted inside the sensitive target.

At the end of the exposure about 906000 frames with (5-20) $\bar{K}$ per frame had been obtained. An ideogram figure 6 of the approximate beam momentum is shown. The total kaon path length is about 1000 km.

The number of frames at each beam momentum is shown in table 2 . The films that have been used for results described in this thesis all come from the 229000 frames exposed to kaons largely at rest.

These films have been distributed among the following collaborating laboratories, Birmingham, Brussels, Durham, University College London and Warsaw University.

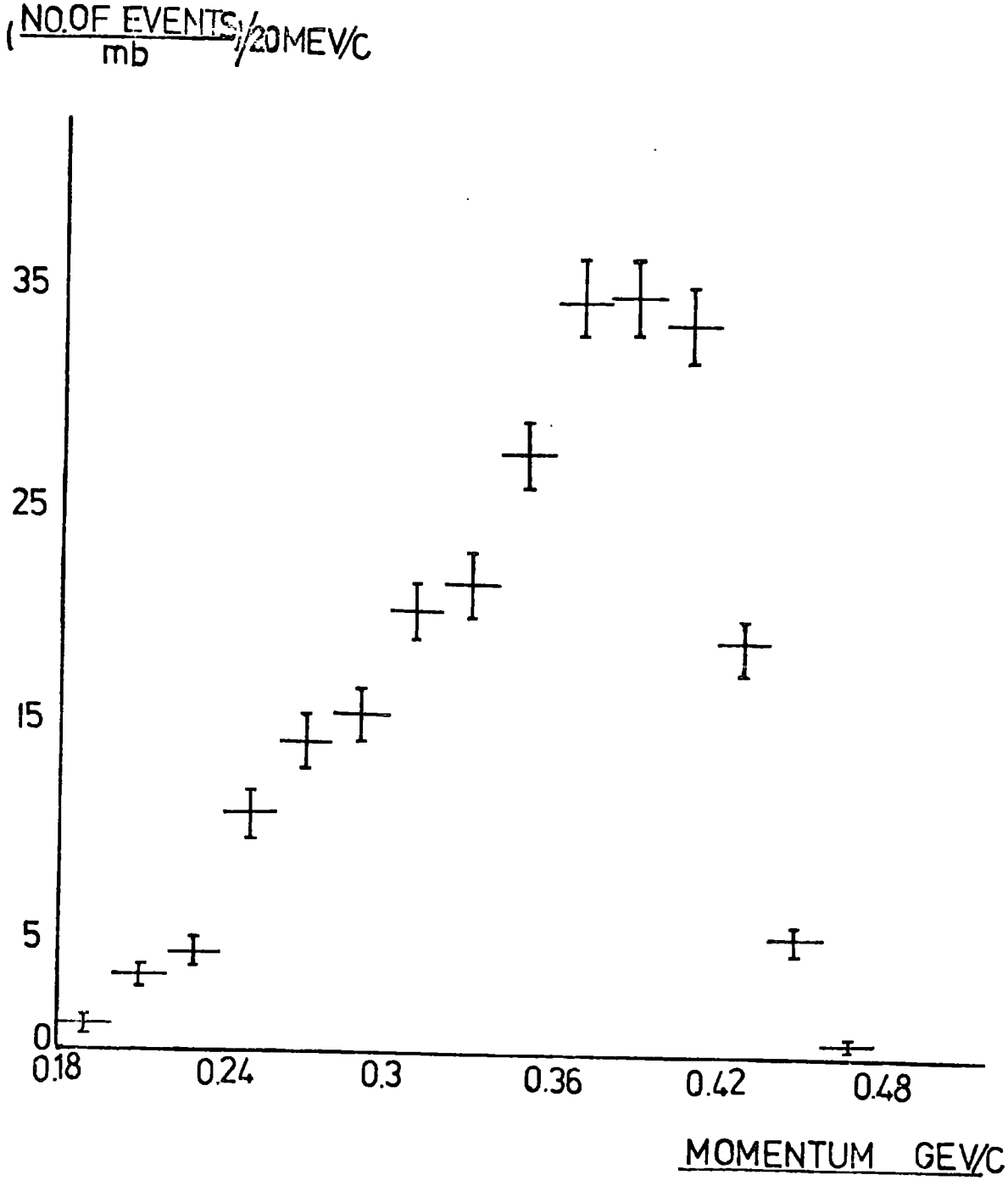

FIG. 6 IDEOGRAM OF APPROXIMATE BEAM MOMENTUM

Table 2

K19 Data taking summary

The experiment was divided into Blocks of film with differing external beam momentum, degrader thickness and target type.

Block No.	Roll Nos.	Thousands of frames	Approx. K^- per frame	Approx. entry momen. MeV/c	Approx. exit momen. MeV/c	Degrader thickness cms. AL	Target frame
1	1-105	229	5	260	0	30	metal
2	106-126	54	8·4	315	235	30	"
3	127-147	45	10·1	370	320	30	"
4	148-168	54	12·3	405	370	30	"
5	169-189	51	8·8	445	410	30	"
6	190-210	52	8·7	320	240	27	perspex
7	211-220	26	7·9	300	190	27	"
8	221-240	51	11·6	370	320	27	"
9	241-250	26	12·2	405	360	27	"
10	251-260	25	10·0	420	380	18	"
11	261-277	44	13·4	450	410	18	"
12	278-286	22	14·2	475	435	18	"
13	287-292	16	17·3	495	455	18	"
14	293-304	28	12·6	505	465	9	"
15	305-314	25	16·6	530	490	9	"
16	315-335	49	20·0	550	510	9	"
17	336-355	49	12·6	560	525	0	"
18	356-365	25	15 7	580	545	0	"
19	366-379	35	15 2	510	475	18	"

Total frames 906000 (229000 for stopping K^-)

CHAPTER THREE SCANNING, MEASURING AND INITIAL DATA

It was emphasised in chapter 1 that the accurate determination of Γ (i.e. Σ^- production/ Σ^+ production at rest) will depend on very efficient scanning and accurate interpretation of events at the scanning table. Only $\sim$ 13% of the events need to be measured.

Since the GEOMETRY and KINEMATICS programmes (see Appendix 1,2) have had to be modified to include the composite chamber and γ rays, and further modifications have had to be made to handle very low momentum primaries it has been necessary to measure considerably more events than envisaged to test out thoroughly the changes that have been made. Despite this the precision of the experiment is still determined at the scanning stage.

3.1 Scanning Procedure

Each charged kaon entering the fiducial volume of the T.S.T. was followed until it either interacted, left the hydrogen volume or left the fiducial volume. The fiducial volume is shown in Figure 7, it is very restricted and ensures that all events recorded will have tracks long enough for accurate measurement. All events of interest were scanned in at least two views. A detailed record was made of the event and great emphasis is placed on accuracy in the scan data since it is largely from these that the Γ ratio is determined.

The classification into events "at rest" or "in flight" has also been made. Each roll of film has been scanned twice by physicists. Any discrepancies between the two scans were resolved in a final check scan.

a) Classification of events

The events found were classified into two broad groups, 0 - prong events and 2-prong events. The 0 - prong events were only recorded if they were accompanied by a K^o decay in hydrogen (for later determination of the charge exchange cross-section in flight), all 2-prong events were recorded and were sub-divided into the following classes:-

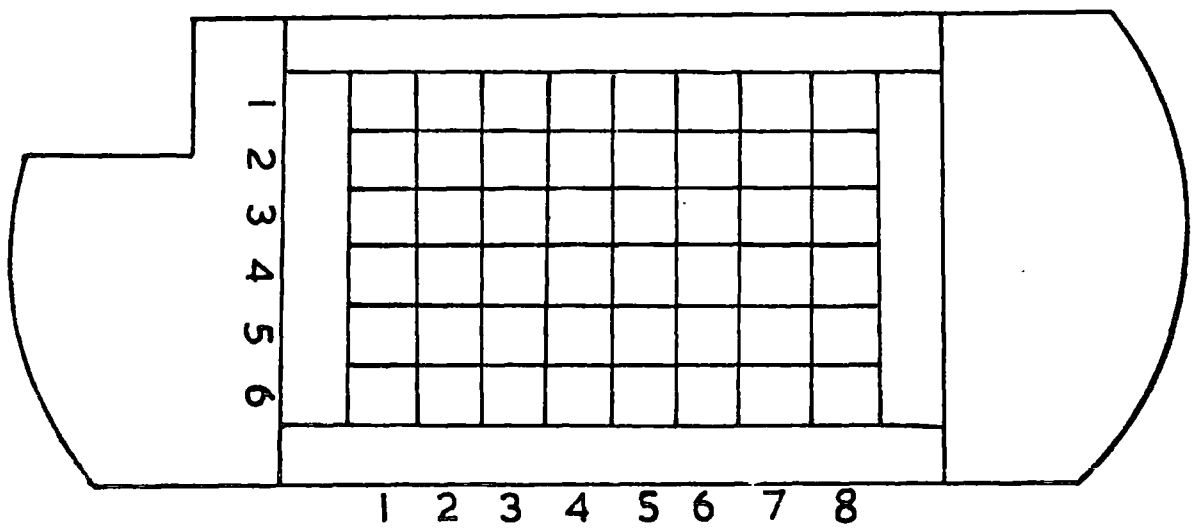

FIG. 7 SCANNING FIDUCIAL VOLUME

1) $K^- P \longrightarrow \Sigma^+ \pi^-$ where the Σ^+ is seen as a visible track and is also seen to decay,

a) to a pion — Σ^+_{π}

or

b) to a proton — Σ^+_p

2) $K^- P \longrightarrow \Sigma^- \pi^+$ where the Σ^- is visible and is seen to,

a) decay to pion — Σ^-_{π}

or

b) to be absorbed — Σ^-_{σ} . If Λ° associated with the Σ^-_{σ} is seen, it is also recorded.

3) $K^- p \longrightarrow \pi^+ \pi^-$ These are events in which the production $\Sigma^{\pm}$ is too short to be seen since it decays almost immediately on production. Because the π^- associated with production and the π^- associated with decay each have momentum in the region of 180 MeV/C, it is largely impossible to classify these events unambiguously into the Σ^+ or the Σ^- channel. Only at momenta above threshold for the charge exchange process can these events arise from the close decay of K° - mesons.

4) $K^- P \longrightarrow \pi^- P$ These may be Σ^+ events where the Σ^+ decays immediately by the proton mode or these are 0 - prong events with the close decay of a Λ° hyperon. Unlike the "$\pi^+ \pi^-$" events, the π^- from Λ° decay has momentum very different from that of the π^- associated with Σ^+ production. Consequently, after measurement by conventional means, or by use of template, at the scan table, these events can be separated unambiguously into the Σ^+ and Λ° categories.

There are possible ambiguities in the classifications Σ^-_σ and π^-p if only scanning information is used. Events classified as Σ^-_σ will comprise those where the Σ^- is identified from the accompanying π^+ meson and where the Σ^- is seen not to decay. These events are largely those in which the Σ^- comes to rest and is absorbed producing a secondary event with neutral secondaries. However, because it is difficult to judge at the scantable, the Σ^-_σ category will include events where the produced Σ^- passes into a plastic window and is absorbed there. To resolve this ambiguity all Σ^-_σ events have been measured. However, as far as the determination of the ratio Γ is concerned it is not necessary to make a separation of the events.

For π^-p events classified as Σ^+_p decays with unseen Σ^+ there may be some contamination from events in which the Σ^+ passes into the perspex and is mistaken for a proton. Some of these may be resolved by the presence of an associated π^+ from Σ^+_π decay. For Σ^+_p the decay proton will come to rest in the plastic window and not be seen.

In determining the value of Γ at rest it is essential to divide the scanned events into those "at rest" and those "inflight". In general all events where the $\Sigma^\pm$ is visible can be unambiguously classified since events at rest all demonstrate accurate collinearity of the $\Sigma^\pm$ and the production $\pi^\pm$. Events in-flight show lack of collinearity except for those events in which the Σ and π are produced at small angles to the direction of flight of the kaon. Then the lorentz transformation leads to a geometry of that event which simulates collinearity. However, from the results of separation into events at rest and in-flight (which occur in a ratio, see later, of about 17.5%) the proportion of in-flight events which can simulate these at rest through collinearity is at most 0.5% of the genuine events at rest. Moreover, events of this kind (i.e. collinearity where Σ and π are produced at small angle to the K) were checked with a template which was

made up of an average profile of kaons coming to rest and producing collinearity at right angles to the kaon track. This proved to be an effective way of separating those events ambiguous between at rest and in-flight. Of course the "$\pi^+\pi^-$" and "π^-p" events can only be judged to be at rest (or in-flight) by use of the template.

b) Recording of scan data through Scan Codes

Events selected as above were recorded as follows. A ten digit number is used with meanings defined as below.

X	Y	A	B	C	D	E	F	G	H

x,y = Zone in fiducial volume where the events is found.

The other digits A to F are zero except for:-

A = prong size of primary vertex

B = 1 for Σ^-

2 for Σ^+

C = 1 for collinearity of Σ and π

= 2 for non-collinearity

= 3 for uncertain collinearity.

D = 1 for proton decay of Σ^+

= 2 for pion decay of $\Sigma^\pm$

= 3 if no decay. This could describe a Σ^- which is absorbed or indeed $\Sigma^\pm$ passing into the perspex window before decaying.

E = 1 for $\pi^+\pi^-$ event

= 2 for π^-p event

F = 1 for associated Λ°

= 2 for associated K°

G = not used

H = 1 if the event is preceded by a 2-prong elastic K scatter.

For example codings for common events produced by kaons at rest are:-

22110000 - $\Sigma^+_p \pi^-$ (collinear)

22120000 - $\Sigma^+_\pi \pi^-$ "

21120000 - $\Sigma^-_\pi \pi^+$

21130000 - $\Sigma_\sigma \pi^+$ (Σ^- without decay)

21130010 - $\Sigma^-_\sigma \pi^+$ (Σ^- absorbed in the reaction $\Sigma P \longrightarrow \mathring{\Lambda} n$)

2000100 - $\pi^+ \pi^-$ event

2000200 - $\pi^- P$ event

The code is invaluable for selecting events from the master list of scanned events on magnetic tape.

3.2 Results of Scanning

Scanning Efficiencies

In order to evaluate the scanning efficiencies, films were scanned twice in this experiment independently. Differences were resolved in a third scan. The events were classified into the following categories:

1 - N_{12} Events found in both scans.

2 - N_1 Events found in the first scan

3 - N_2 Events found in the second scan

4 - N_T True (unknown) number of events on the films.

If λ_1 and λ_2 are the individual scanning efficencies as defined by the expressions

$$\lambda_1 = N_1/N_T \quad \text{and} \quad \lambda_2 = N_2/N_T \qquad \ldots\ldots\ldots\ldots\ldots\ldots(29)$$

Then $\lambda_1 \cdot \lambda_2$ is the probability that an event will be seen in both scans. Then:-

The number of events found in both scans is

$$N_{12} = \lambda_1 \cdot \lambda_2 \cdot N_T \qquad \ldots\ldots\ldots\ldots\ldots\ldots(30)$$

solving equations (29), (30)

$$\lambda_1 = N_{12}/N_2 \,, \quad \lambda_2 = N_{12}/N_1 \qquad \ldots\ldots\ldots\ldots (31)$$

and

$$N_T = N_1 \cdot N_2 / N_{12} \qquad \ldots\ldots\ldots\ldots (32)$$

The probability that scanners 1, and 2 will both miss an event should be given by:

$$q = (1-\lambda_1)(1-\lambda_2) \qquad \ldots\ldots\ldots\ldots (33)$$

Then the combined efficiencies over two scans should be

$$\lambda_C = 1-(1-\lambda_1)(1-\lambda_2) \qquad \ldots\ldots\ldots\ldots (34)$$

$$= \lambda_1 + \lambda_2 - \lambda_1 \cdot \lambda_2$$

3.3 Measurement of events

The measurements were carried out on image plane digitized machines where the accuracy, corresponding to helix fit errors on the film was about 8μ for track measurements and about 10μ on fiducial cross measurements. Because small angle scattering of the primary kaon is quite probable, 15 points were measured on each primary to detect scattering. Such primaries are failed by the on-line measuring system and so the primary track has to be reduced in length to remove the scatter and measured until the primary is accepted. In this way a scattering was not allowed to bias the measured curvature of the track. A scattering very close to the primary interaction would lead to the event becoming unmeasurable.

The measurements were processed by the GEOMETRY and KINEMATICS programmes which had been modified:-

a) to take account of the geometry of the T.S.T. system and the measurement of γ rays (reference 13).

b) to allow for fitting of events in KINEMATICS where the primary is stopping (reference 14). If the measured momentum of the K primary is in excess of 50 meV/c, then standard KINEMATICS

is used. Below this momentum, the fitting routine of KINEMATICS is modified to take into account the increasing lack of dependence of the momentum of the vertex on the measured momentum of the midpoint of the track.

The pass rate in GEOMETRY is about 80% and in KINEMATICS a further 80%, leading to an overall pass rate of about 64%. After measurement, events which have failed were re-examined (judged) on the scan table to decide if the event should be remeasured. The main category of failures comprised events with short straight tracks which result from the shallow depth of the T.S.T. In all there were 3 passes of the unsuccessful events through the measuring/processing chain. The total, overall pass rate from measurement through to KINEMATICS is 98%. The scanning/measuring sytem is summarised in figure 8. Two groups of measurements were made.

i) The first of these consisted of all $\pi^+\pi^-$ and π^-p events. Here the aim of the measurement was to

   a) check the division of these events into "at rest" and "in flight" categories previously judged by the template,

   b) to resolve these π^-p events, which were not resolved by template, into Σ^+ and Λ categories.

ii) The second group comprised all events judged to be in-flight to provide data for the cross-sections of in-flight interactions and particularly for the variation of the quantity Γ with energy.

3.4. Results of measurements

a) General results on beam momenta

Beam momenta can be determined at two stages. The first is at the end of the GEOMETRY programme where the momentum corresponding to the helix fitted to the measured points is available. The second is at the end of KINEMATICS where if this momentum has been "pulled" to a new value with

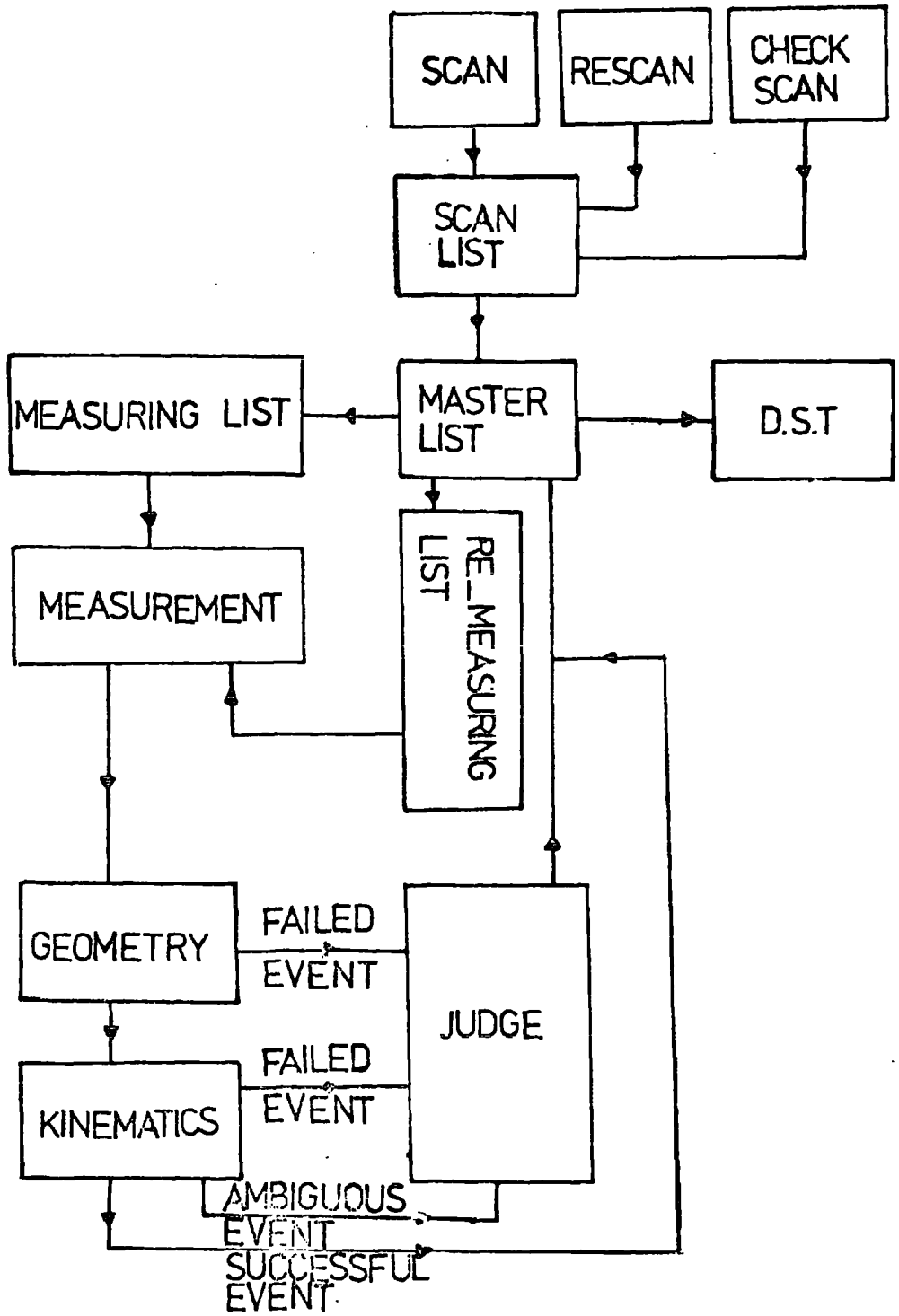

FIG. 8 EVENT PROCESSING CHAIN

higher precision by the fitting procedures.

Since the "pulling" in the fitting procedures varies with the tightness of the constraints in the fitting, then for example, a comparison of $\pi^+\pi^-$(unconstrained fits) with Σ^+_{π} (highly constrained fits) should be made at the end of GEOMETRY and not after KINEMATICS. The reasons for this are quite clear in the figures below.

i) Collinear events (Σ^-_{π} , Σ^+_{π} and Σ^+_{p})

The distribution of beam momentum is expected to be close to zero momentum for these collinear (hence stopping kaon) events. As can be seen in figure 9 the beam momentum after GEOMETRY shows a spike at zero momentum which corresponds to all primary kaons whose measured momentum at the midpoint of the track is less than that expected from the range of the track ("overstopped" kaon). There is a second group distributed about 100 Mev/c. When these events pass through the fitting routines of KINEMATICS the momentum is pulled as expected towards zero.

This is clearly seen in figure 10. In general these fitted momenta are less than 50 Mev/c and certainly less than 100 Mev/c.

ii) Non-collinear events (Σ^-_{π} , Σ^+_{π} , and Σ^+_{p})

The non-collinearity of these events implies that they are not at rest. The beam momentum from GEOMETRY figure 11 is now distributed about 200 Mev/c, that from KINEMATICS, figure 12 no longer shows the pulling towards zero momentum.

iii) At rest and in flight events ($\pi^-\pi^+$ and π^-p)

The distribution of beam momentum from GEOMETRY, figures 13,14, is now little different from that from KINEMATICS although these events do fit the unphysical (strangeness not conserved) channels $\pi^+\pi^-n$ and $\pi^-p\pi^0$. This is because the degree of constraint is low. However it is clear from a comparison of figures 10, 12,13,14 that this group of data contains both 'at rest' and 'in flight' interactions.

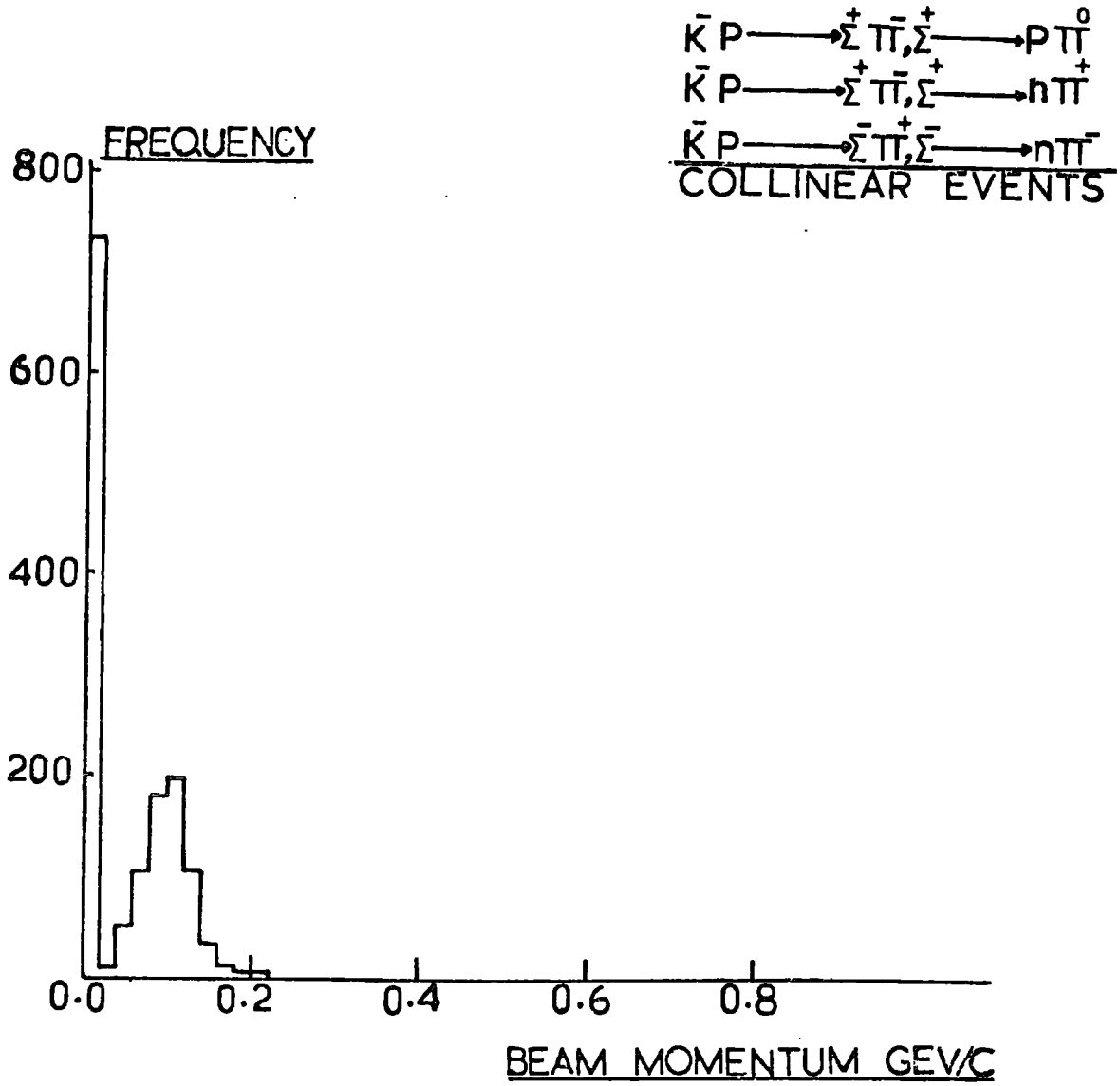

FIG. 9 UNFITTED BEAM MOMENTUM DISTRIBUTION

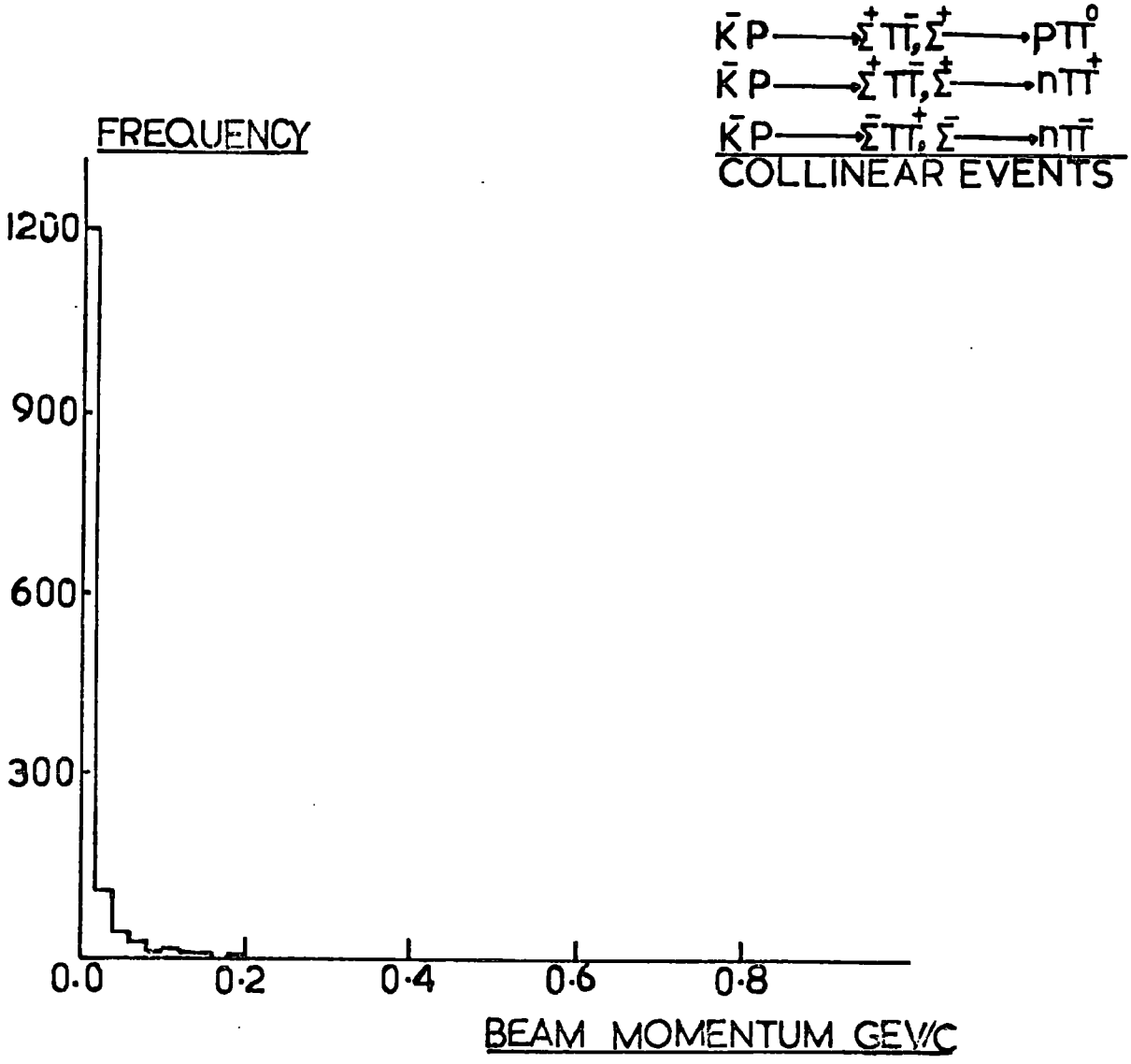

FIG. 10 FITTED BEAM MOMENTUM DISTRIBUTION

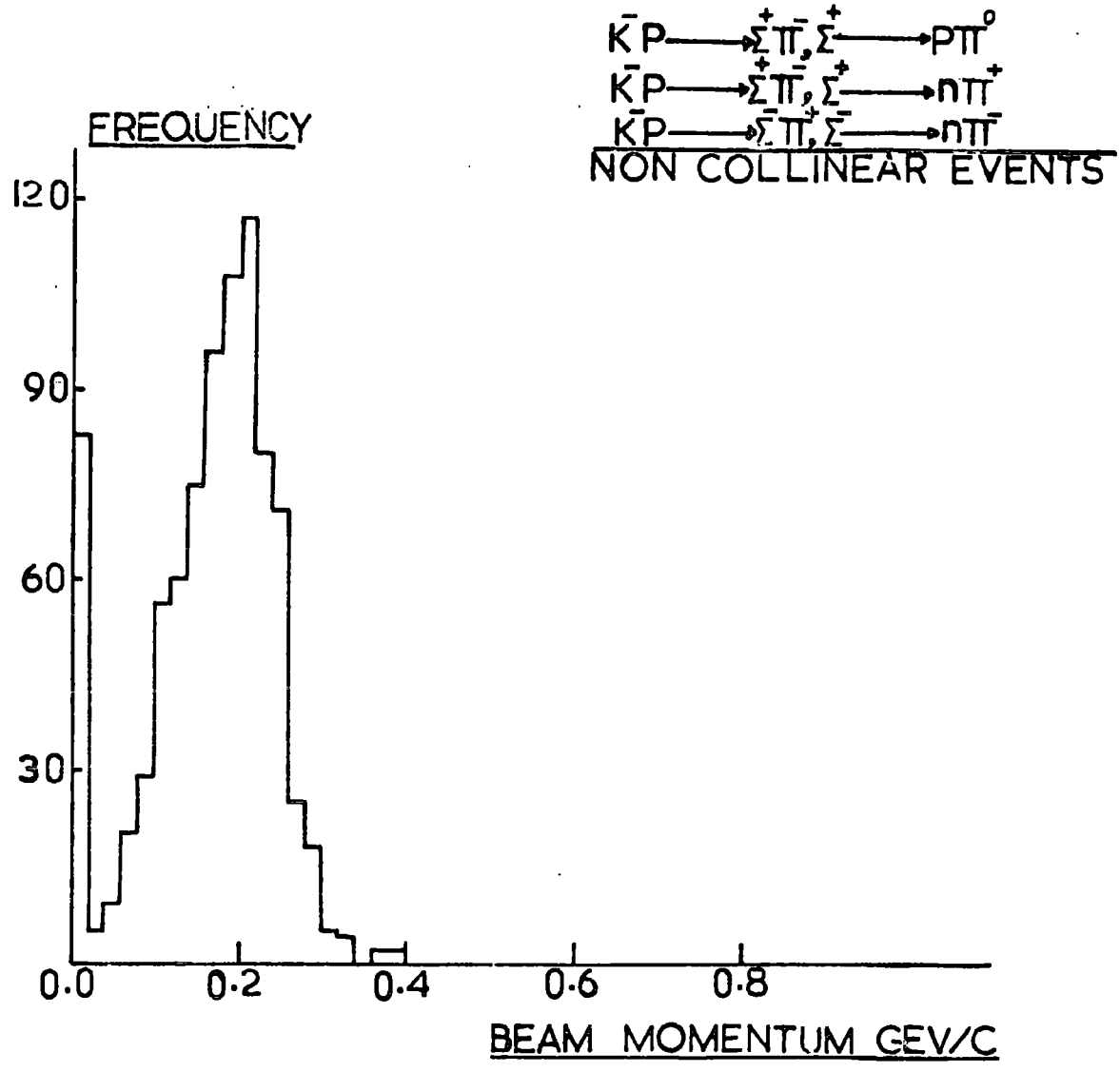

FIG.11 UNFITTED BEAM MOMENTUM DISTRIBUTION

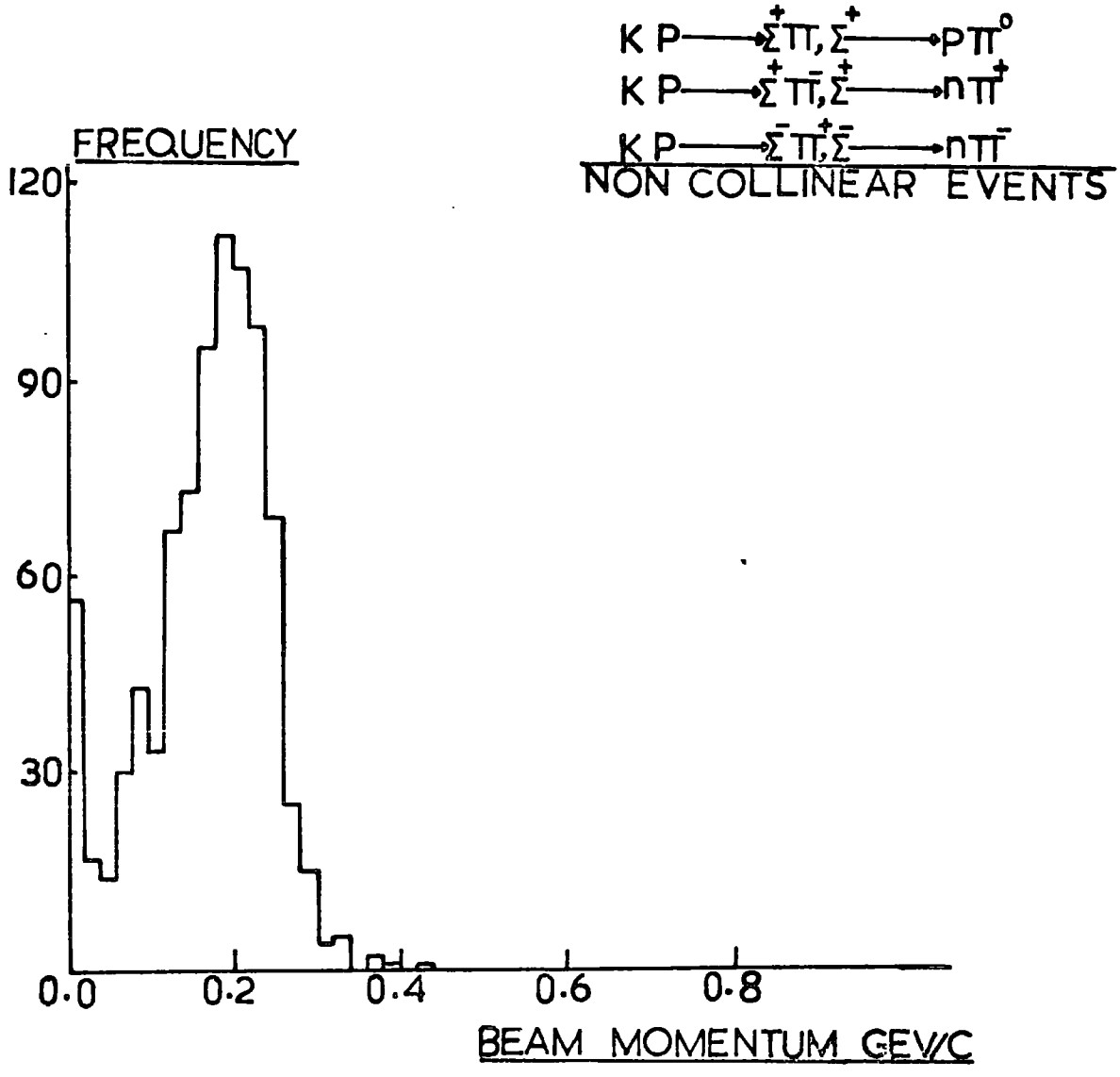

FIG. 12 FITTED BEAM MOMENTUM DISTRIBUTION

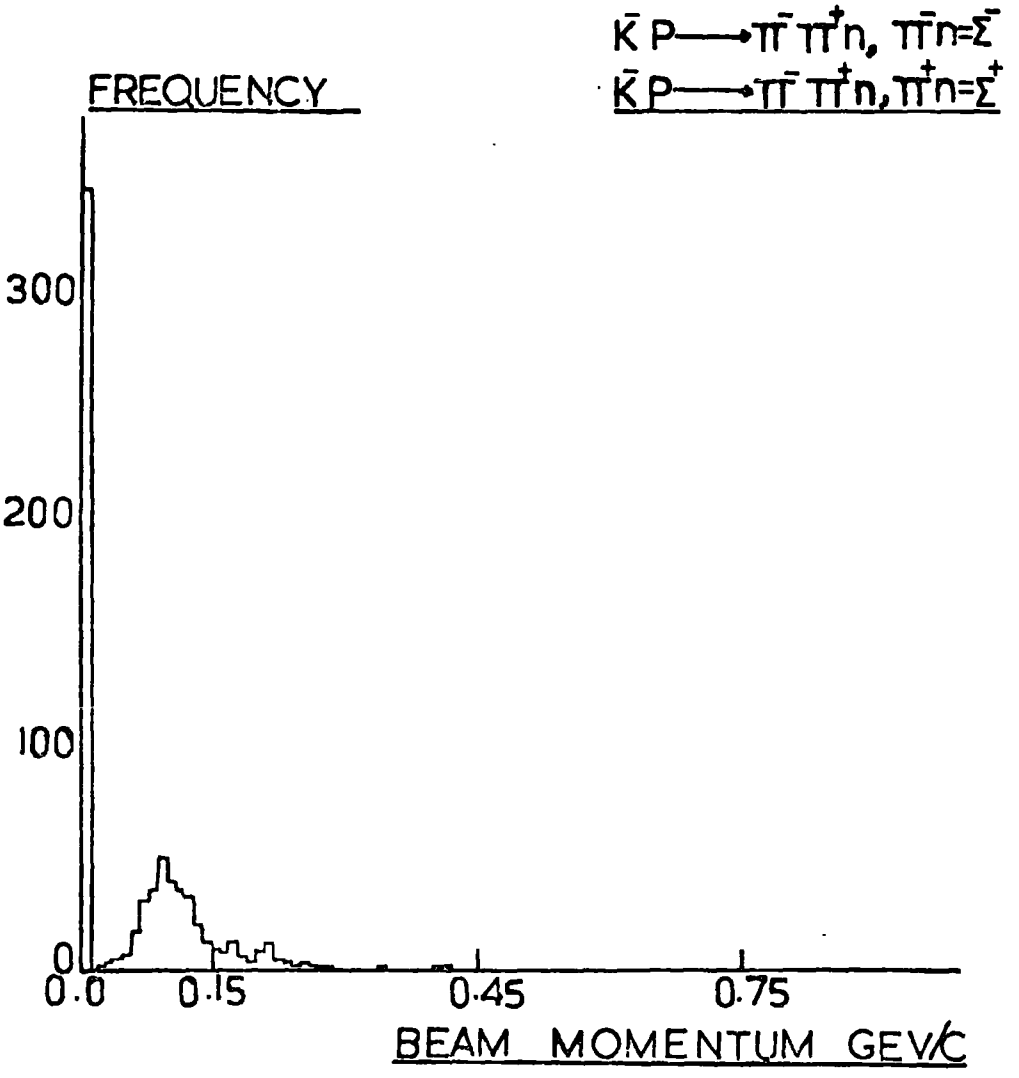

FIG. 13 UNFITTED BEAM MOMENTUM DISTRIBUTION

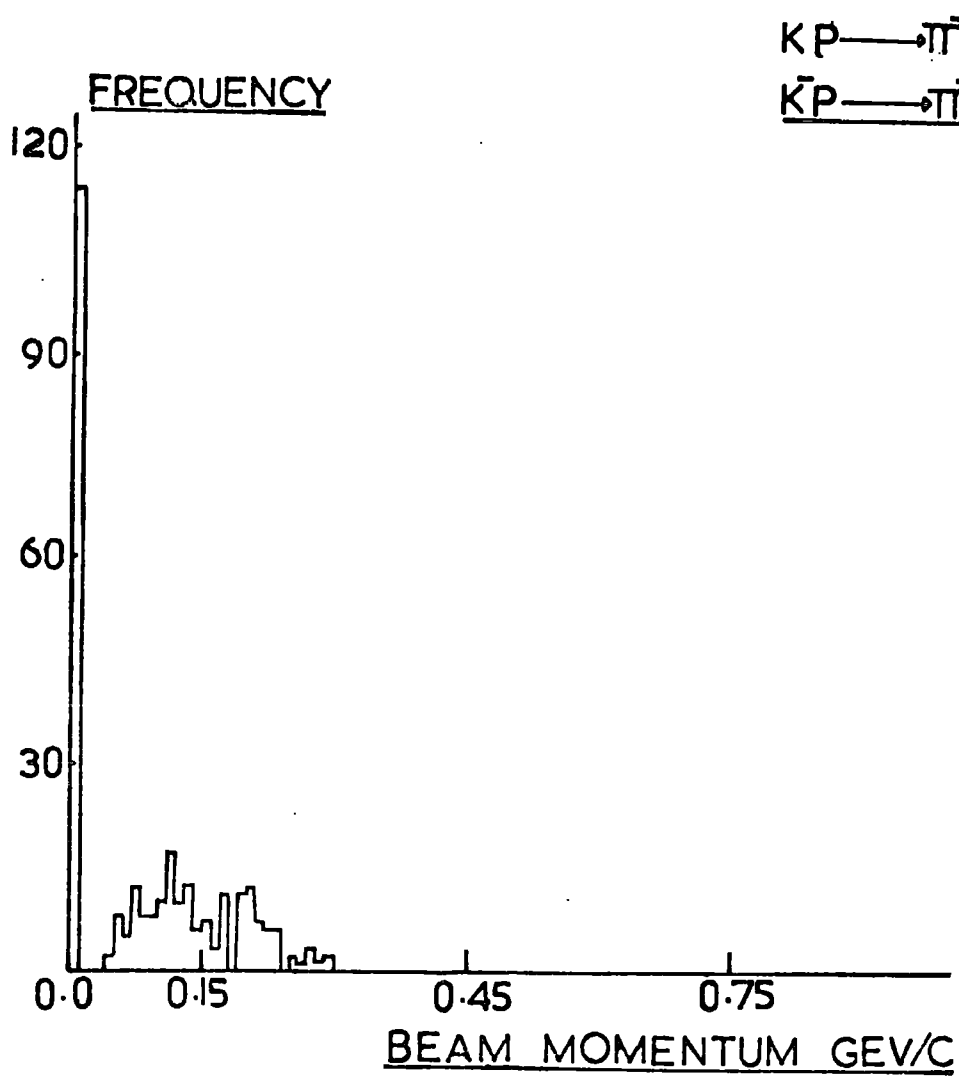

FIG. 14 UNFITTED BEAM MOMENTUM DISTRIBUTION

b) Resolution of $\pi^+\pi^-$ and π^-p events into the "at rest" category

To separate the "at rest" group a comparison is made of the distribution of beam momentum with that for collinear events. Each shows a spike of zero. It has to be assumed that this spike corresponds to primaries which are exactly at rest. Normalising to the collinear events, then the number of "at rest" $\pi^+\pi^-$ (or π^-p) events whose measured momenta are in the region of $\sim$ 100 Mev/c can be calculated. The difference between the calculated and observed values is the number of events in-flight.

It is clear from figure 11 for non-collinear (in-flight) events, that although the primaries interact in-flight, the distribution of measured momenta shows a spike at zero momentum. Correspondingly the assumption made above in normalising the spikes of collinear and $\pi^+\pi^-$ or (π^-p) events is not completely valid. This will have lead, above, to an over-estimation of the number of $\pi^+\pi^-$ (or π^-p) events at rest.

A separation has also been made by using a template to judge whether the primary is at rest. The template was checked against collinear and non-collinear events which suggests that at most 2% of those primaries judged to be at rest are in fact in-flight.

Both methods of judging at rest events are compared in tables (3 and 4). Because of the uncertainty of the first method, judgement of "at rest" by template is preferred and this method only is used subsequently.

c) Resolution of π^-p into Λ° and Σ^+ categories

Whereas the use of a template appears to be the best method of resolving whether the primary of an interaction was at rest or in-flight, this does not appear to be so for judging whether a π^-p event is due to the production and decay of a very short-lived Λ° or Σ^+.

In principle the momentum of the negative pion produced in association

COMPARISON BETWEEN EVENTS AT REST AND IN FLIGHT USING

a) Template

TABLE. 3.

$TT^{+}T\bar{T}$ (TOTAL SAMPLE) =822		$T\bar{T}P$ (TOTAL SAMPLE) =406	
AT REST	IN_FLIGHT	AT REST	IN_FLIGHT
84.9%	15.08%	71.8%	28.8%

b) Measurement

TABLE. 4.

$TT^{+}T\bar{T}$ (TOTAL SAMPLE) =701		$T\bar{T}P$ (TOTAL SAMPLE) =289	
AT REST	IN_FLIGHT	AT REST	IN_FLIGHT
94.9%	5.04%	76.5%	23.47%

with the Σ^+ or in the decay of the Λ° is sufficient to resolve these categories. For example, the momentum of the produced pion is about 180 Mev/c for the Σ^+ and is below 140 Mev/c for the Λ°. Templates drawn to curvatures corresponding to these momenta should lead to adequate resolution where there is sufficient pion length, discrimination by the template is possible but this occurs in approximately 63% of the events.

For the remainder, although the track length is too short for resolution by template, measurement leads to the separation of events.

In a sample of about 55% of all $\pi^- P$ events (judged to be at rest) that were measured it is possible to estimate the proportions which are due to Σ^+ and to Λ. The events are plotted in figure 15 where for each event the pion momentum and the opening angle between the pion and the proton are shown. The data divide clearly into two groups, one centred on the expected momentum of 180 Mev/c for Σ^+ and the other clustered about the kinematically expected relation between the pion momentum and opening angle for the relation for the reaction $K^- P(\text{at rest}) \longrightarrow \Lambda \pi^\circ$. The corresponding relation for the reaction $K^- P \longrightarrow \Sigma^\circ \pi^\circ$ leads to lower pion momenta. From this plot the proportion of events due to Σ^+ decay is estimated to be ($73 \pm 7.9\%$). This figure is then applied to the whole sample.

A small number of the so-called $\pi^- P$ events arise in fact from $\pi^- \Sigma^+$ events where the short Σ^+ passes into the target wall decays there. For pion mode of decay the probability that the pion emerges from the wall is estimated, by Monte Carlo calculations, to be as high as 95%. Prior to the measurements above all of the so-called $\pi^- P$ events were scrutinized and 10 were found to have associated pions. These have been transferred to the Σ^+_{π} class.

d) Σ^-_{σ} events

These events were measured for two purposes. One is to determine the range of the absorbed Σ^- since this will provide a check on the range momentum relation that is used in GEOMETRY and KINEMATICS. The second

π^-p EVENTS AT REST (BY TEMPLATE)

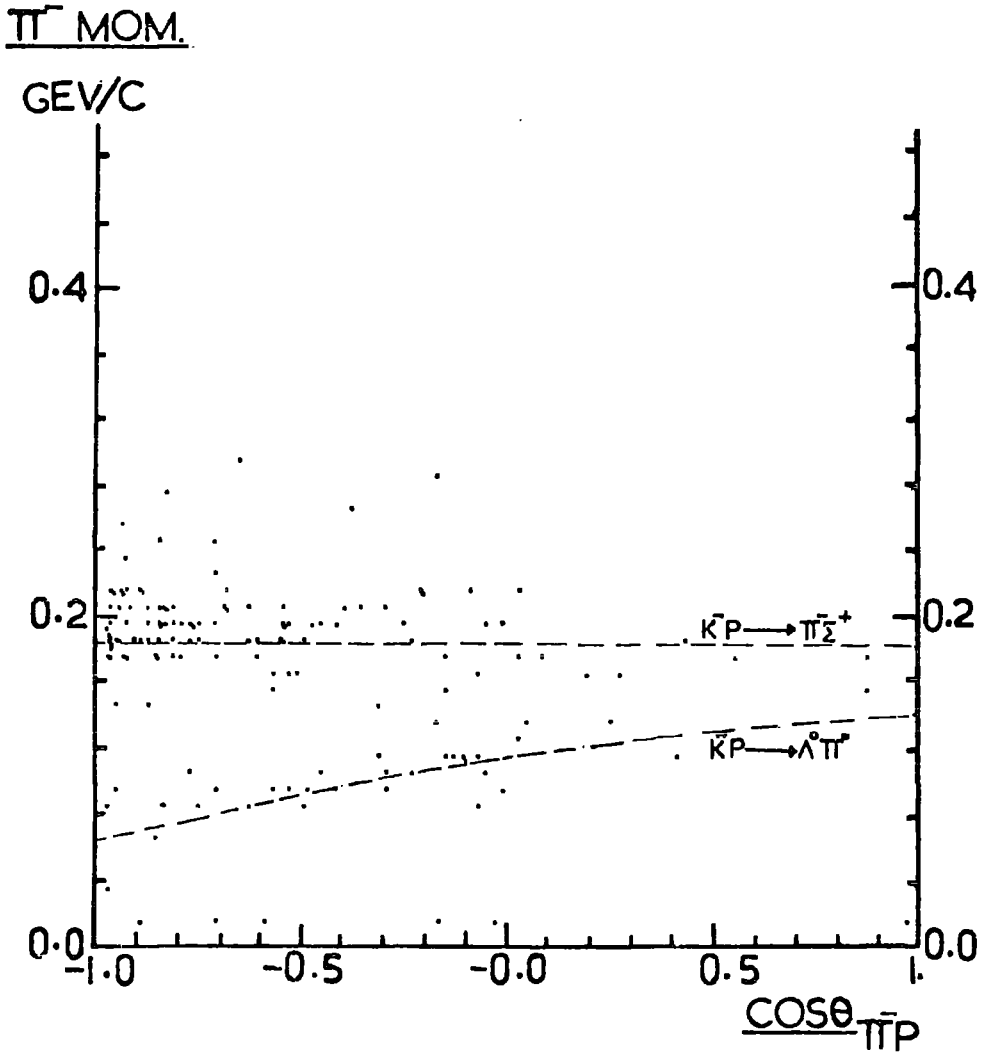

FIG.15. MOMENTUM OF NEGATIVE PION AGAINST THE OPENING ANGLE BETWEEN THE PION AND THE PROTON

purpose is to determine, what proportion of the events were due to the Σ^- entering the plastic.

The average range if found to be (1.19 ± 0.05) cm and this confirms the correctness of the range momentum tables used. The number of events terminating in the perspex is found to be about 8%. As pointed out in section 3.1.a these terminating events do not affect the determination of Γ.

3.5 Final classification of events

To summarise, events have been classified into at rest and in-flight largely by the collinearity of the events and in a small number of cases by the use of a template. These events have been further divided into physical channels. In a relatively small number of cases measurements have been used to resolve ambiguities. The results of the scanning and the classification of the data produced in Durham are shown in detail in table 5. The scanning efficiencies from a double scan (plus a check scan) are all found to be high. These events together with the events from the collaborators at Brussels, UCL, and Warsaw are gathered together and discussed in chapter 4.

RESULT OF SCANNING

TABLE. 5.

CLASSES	AT REST&INFLIGHT		AT REST		INFLIGHT	
	TOTAL NUMBER OF EVENTS	EFFICIENCIES	TOTAL NUMBER OF EVENTS	EFFICIENCIES	TOTAL NUMBER OF EVENTS	EFFICIENCIES
$\bar{\Sigma}_{\pi}$	4856	97.91	4271	99.95	585	99.96
$\bar{\Sigma}_{o}$	643	97.89	560	99.94	83	99.95
Σ^{+}_{π}	1290	97.91	1035	99.95	255	99.96
Σ^{+}_{p}	1229	97.81	1010	99.95	219	99.86
$\pi^{+}\pi^{-}$	822	97.51	698	99.84	124	99.67
$\pi^{-}p_{(\Lambda)}$	1234	94.9	93.4	994	30	97.46
$\pi^{-}p_{(\Sigma^{+})}$	291.6		204.6		87	
K^{o}	140					89.25

THE TOTAL EFFICIENCY FOR AT REST SAMPLE=99.93

THE TOTAL EFFICIENCY FOR INFLIGHT SAMPLE=99.967

CHAPTER FOUR DETERMINATION OF THE $\bar{\Sigma}/\Sigma^+$ PRODUCTION RATIO AND THE Σ^+ DECAY BRANCHING RATIO

4.1 Total available data

Altogether in the collaboration between the groups of Brussels, Durham, University College London and Warsaw about22354 events have been found by careful scanning and check scanning. A breakdown of the total data is presented in table 6 in two forms.

Firstly the data is presented in the form for use in method 1, which is the method which relies largely on the accurate identification of the proton mode of decay of the Σ^+ but not on the separation of the pion modes of decay of the Σ^+ and Σ^-. A subset of these data was scanned in which the separation of the pion modes was pushed to its limit. This means that events were further scrutinized and separated into Σ^+ and Σ^- categories. These data were used in method 2. All the data have been corrected for scanning efficiency and in flight events as in table 5.

4.2 Determination of Γ

The two methods referred to above have been described in detail in chapter 1. In the first of these the branching ratio of the pion and proton modes of decay of the Σ^+ is assumed in determing Γ, in the second, both the branching ratio and the value of Γ are determined.

a) Method 1

The advantages of this method are:-

(1) It is independent of the separation of $\pi^+\pi^-$ events into those from Σ^+ and from Σ^- hyperons respectively.

(2) It is independent of the mistaken classification of Σ^- events as Σ^-_o events.

(3) That the precision depends upon the number of Σ^+_p events. These are readily identifiable at scanning time.

FINAL RESULT FROM THE COLLABORATION

TABLE 6.

DATA FOR METHOD 1

CLASSES	$\Sigma^-_\pi + \Sigma^+_\pi + \Sigma_\sigma + \pi^+\pi^-$	Σ^+_p	TOTAL
NUMBER OF EVENTS	18905	3449	22354

DATA FOR METHOD 2

CLASSES	Σ^-	Σ^-_σ	Σ^+_π	Σ^+_p	$\pi^+\pi^-$	TOTAL
NUMBER OF EVENTS	8505.5	1070.1	1862.8	2216.6	948.9	14603.9

Then the total number of Σ^- – hyperon produced by kaons is

$$N^- = N_{\Sigma_\sigma}(obs) + N_{\Sigma_\pi^-}(obs) + N_{\Sigma_\pi^+}(obs) + N_{\pi^-\pi^+}(obs) - \frac{B(N^+)}{1-B} \quad \ldots\ldots (22)$$

and the total number of Σ^+ – hyperon is

$$N^+ = \frac{N_{\Sigma_P^+}(obs) + N_{\pi^-P}}{1-B} \quad \ldots\ldots (16)$$

Using the number given in table 6a and the branching ratio, B, from the Paricle Data Group Tables ($B = 0.4835 \pm 0.007$), ratio Γ is just N^-/N^+ and is found to be

$$\Gamma = (2.35 \pm 0.07)$$

b) Method 2

Table 6b shows the numbers of events in the scanning channels used in this determination of Γ. These numbers include the corrections which were discussed in sections 3.3. and 3.4. No events have been rejected by selection criteria. In this method, it is assumed that the ability to distinguish the sign of the charge of a Σ – hyperon should depend only upon whether the Σ track can be resolved, so that the recoil pion can be identified and its charge determined. If the short distance, r, is defined as the minimum effective length needed to detect the charge of the hyperon then the number of Σ^- hyperons decaying by the pion modes in a distance r and which will appear as $\pi^+\pi^-$ events is shown by equation 27. (see chapter 1 and below). From the numbers of $\pi^+\pi^-$ events in table 6b the cut off length r can thus be determined. When it, and other data from table 6b, are substituted into equations 25 and 28 then the Γ ratio and the branching ratio B of the Σ^+ can be determined:

$$N(r) = (N_\sigma^- + N_\pi^-)(e^{t^-(r)/\tau^-} - 1) + N_\pi^+(e^{t^+(r)/\tau^+} - 1) \quad \ldots\ldots (27)$$

$$\Gamma(r) = \frac{(N_\sigma^- + N_\pi^-)(e^{t^-(r)/\tau^-})}{N_p^+ + N_\pi^+(e^{t^+(r)/\tau^+})} \quad \ldots\ldots (25)$$

$$B = \frac{N_{\pi}^{+} \, e^{t^{+}(r)/\tau^{+}}}{N_{p}^{+} + N_{\pi}^{+} e^{t^{+}(r)/\tau^{+}}} \qquad \ldots\ldots\ldots\ldots (28)$$

The above equations allow, by interpolation, to find the effective range, r, which applies to the scanning of this experiment and the values of Γ and B.

These values are:

$$r = 0.045 \text{ cm}$$
$$\Gamma = 2.38 \pm 0.04$$
$$B = 0.487 \pm 0.008$$

4.3. Critique of methods for Determining Γ

A summary of the previous determinations of Γ is given in table 7. Only those of Kim, Tovee and the present work are of sufficient precision to warrant further discussion. Superficially, previous methods which have used bubble chamber and nuclear emulsion techniques to determine Γ are similar. In both, events are selected for analysis which are judged to be the production of $\Sigma^{\pm} \pi^{\mp}$ in kaon interaction at rest on proton because the tracks of the produced $\Sigma \pi$ particles are collinear. However the composition of the events, as seen below, differ considerably and in these differences the disparity of the measured values of Γ must lie.

In the chamber the potential ranges of the produced $\Sigma^{\pm}$ hyperons are about 1.05 and 1.26 cm respectively. As these are long compared to the decay lengths then about 93% of the Σ hyperons decay in flight. If the decay occurs in the first 0.5 to 1mm of the path of the Σ, the hyperon is not seen. A correction for the loss of events over the short, but not very well known, distance has to be made. The effect of measuring error on this small distance leads to over correction where the lifetime is very short. Consequently the measured value of $\Gamma = \Sigma^{-}/\Sigma^{+}$ will be reduced.

In the emulsion there is no magnetic field to determine the sign of the charge of the Σ – hyperon. However with potential ranges of 0.06 to

TABLE(7)

DETERMINATION OF THE Σ^-/Σ^+ PRODUCTION RATIO BY K MESON CAPTURES AT REST

Author	r
Humphrey and Ross (ref: 2)	2.15 ±0.12
Kim (ref: 1)	2.06±0.06
Eisele (ref: 8)	2.2 ±0.1
Value deduced from Chang's data (ref: 7)	2.29±0.11
Tovee (ref: 5)	2.34±0.08
This experiment	2.35±0.07

0.08cm most hyperons (about 82%) come to rest where the signatures for charge are clear (Σ^- hyperons are absorbed, Σ^+ hyperons decay collinearlly into protons of characteristic range or into pions of characteristic ionisation). Consequently only those Σ hyperons can be employed in the analysis which have stopped and a correction for the approximately 18%, events in flight has to be made. In this case the distances over which the corrections are to be made are quite precise, and relating these distances to proper times is also precise.

On balance the emulsion method is freer of systematic effects than previous bubble experiments and hence the result of Tovee is to be preferred to that of Kim. This conclusion is fully supported by the work described in this thesis which is independent of lifetime correction. It relies heavily on the classification of events at scanning time and hence calls for high scanning efficiency and judgement.

A further indication that the Kim value is in error is provided by an analysis of A.D.Martin (reference 15) who has carried out a determination of the coupling constant $g_{KN\Lambda}$ and $g_{KN\Sigma}$ by means of relating KN amplitudes by dispersion relations. An important conclusion is that the low momentum data (provided almost entirely by Kim) is probably in error by as much as 20%.

The advantage of the present methods is that selection criteria (such as those quoted by Eisele have been avoided and consequently their associated systematic effects do not feature in the final results. However, it should be pointed out that in method 2 the effective length, r, that is determined is effective in two senses. Firstly there is no absolute cut off length but a spectrum of lengths which vary with the geometry of the events and with observers. Secondly, this effective length is non physical in that, it is cut off length corresponding to zero measuring errors (see table 1). In other words above this length all events are resolved, below they are not.

In method 1 the difficulties above are avoided but the method relies heavily on identifying Σ^+_p decays. The majority of these where the Σ itself is visible, present no problem at all and are already separated from Σ^+_π decays by the ionisation of the decay particle. However, it was discussed in chapter 3, these events are contaminated by events where Λ hyperons decay close to the production vertex.

Although the resolution of these events is good, any Λ decay left in the sample will lead to a reduction of Γ .

4.4 Summary

It has been seen above that the determination of Γ and B are consistent with one another. Compared to the two previous determinations of Γ (with good statistics), it is clear that the present result is in good agreement with the value of Tovee but not that of Kim. By taking a weighted average of the Tovee value and the value in this thesis the following value of Γ is obtained:

$$\Gamma = (\quad 2.35 \pm 0.05 \quad)$$

The value of the branching ratio,B, for the Σ^+ hyperon determining above (0.487±0.008),represents a new determination of this quantity with a precision close to the existing world value. The closeness of our values of B to the world value gives confidence in the determination of Γ value.

APPENDIX ONE

GEOMETRY Programme

The T.S.T. contains hydrogen whilst the main chamber volume is fitted with a mixture of neon and hydrogen. A geometrical programme HGEOM had been modified by (J.Guy) to reconstruct the tracks in the chamber and to allow for the extra media, consequently Range-momentum tables had been generated for the three media (hydrogen,perspex and neon-hydrogen). Other constants such as that for the coulomb scattering in the perspex must be provided and storage allocated in the geometry programme.

The track which leaves the hydrogen and goes into the neon is indicated by measuring the last point in hydrogen twice. However helix fittings were applied to the track sections so as to reconstruct them separately. Meanwhile a check was made to see if the track has crossed the perspex plane and returned into hydrogen. If so the second part of the track is ignored.

HGEOM provides centre of track variables ($1/p, \phi, \tan\lambda$) and their correllated errors which are the normal measured quantities used by the KINEMATIC fitting programme HKIN, further for the neon section of the track these 3 variables are swum to the mid point of hydrogen and a mean of these variables and those for hydrogen is taken. When the geometrical reconstruction of the bubble chamber event has taken place, the event must be tested against hypotheses of the nature of the event suggested by the experimenter. (KINEMATICS).

APPENDIX TWO

KINEMATICS Programme

By using the conservation laws of energy, momentum, charge....etc. the KINEMATIC programme attempts to identify uniquely the tracks for the reconstructed events.

Modification had been made to the KINEMATICS Programme to handle stopped K events. Fitting stopped K with ordinary KINEMATICS (i.e. the version used for in-flight fitting events) leads to a low pass rate e.g. on a sample of sigma-pion events, a pass rate of about 65% through KINEMATICS was obtained.

It is necessary to have a reliable fitting system in order to separate events at rest from those at low momentum (e.g. 100Mev/c) which have been essentially separated by template . A version of KINEMATICS fitting to Px, Py, Pz at the vertex instead of the variables ϕ , $\tan\lambda$, $1/p$ was introduced into subroutine ITERAT and this lead to a high pass rate, but also so difficult interpretation of the quality of the fits since the input errors are not Gaussian. However, the fitted values of K-momentum at the vertex did not show an improvement over the measured values. Moreover altering the constraint tolerances in the fitting did not lead to any effective improvement.

A further modification was made in fitting at rest events, such that standard KINEMATICS could be used. The variation of centre of track momentum depends on the change in vertex momentum through the range momentum relation and so the fitting routine of KINEMATICS was modified to take into account the increasing lack of such dependence at low momentum with an arbitrary function. The Swim routine was modified so that when the vertex momentum of the K is less than 50 Mev/c, the normally returned vertex slope is multiplied by the arbitrary function which is unity at p = 50 Mev/c and zero for P= 0 Mev/c. Results of modification to pass

rate was similar to those obtained from Px, Py, Pz but the stretch functions are now Gaussian and the fitted K-momentum distribution gives a much sharper peak at zero.

ACKNOWLEDGEMENTS

I would like to thank Professor A.W.Wolfendale who made available the facilities of the Physics Department at Durham during my work for this thesis. My particular thanks go to my supervisor, Dr.J.V.Major for the enormous amount of help and useful advice he has given and the many interesting discussions we have had.

I would like to thank all the other members of the Higher Energy Nuclear Physics Group at Durham for their many discussions during the course of the work, particularly Mr.N.H.Bedford. I am grateful to the staff of the collaborating laboratories, particularly, Professor J.A.Zakrzewski and Mr.J.Ciborowski.

My thanks are due to all the Scanning and Measuring Staff at Durham University for their work on this experiment.

Lastly, but by no means least, I would like to thank my parents, without their grants during my stay in England to study, this thesis would not have been possible.

REFERENCES

Chapter One

1 J.K.Kim thesis, Columbia University (1966), (unpublished)

2 W.E.Humphrey and R.R.Ross, Phys.Rev.127, 1305 (1962)

3 R.H.Dalitz and S.F.Tuan, Ann.Phys.(New York) 10, 307, (1960)

4 A.D.Martin. Springer tracks in Mod.Phys.55 (1970), 142

5 D.Tovee, D.Davis, J.Simonovic, G.Bohm, J.Klabuhn, F.Wysotzki, M.C.Seithey-Barth, J.Wickens, T.Cantwell, C.Nighogain, A.Montwill, K.Garbowska-Priewska, T.Priewski and J.Zakrewski, Nucl.Phys.B33 (1971) 493.

6 M.Sakitt, T.B.Day, R.G.Glasser, N.Seeman, J.Friedman, W.E.Humphrey and R.R.Ross, Phys.Rev.139, 719, (1965)

7 C.Y.Chang, Phys.Rev.151 ,1081 (1966)

8 F.Eisele, H.Fitthuth,V.Hepp,W.Presser and G.Zech,2.Physick 238,37e, (1970)

9 Particle Data Group (A.Rittenberg, A.Barbar-Galtieri, T.Lasinski, A.H.Rosenfeld, T.G.Trippe, M.Roes, C.Bricman, P.Soding, N.Barash-Schmidt and G.G.Wohl),Rev.Mod.Phys. 43 part II, Si, (1971)

Chapter Two

10 C.M.Fisher. External Report. RL - 73-053

11 K.A.Kamakhy. Durham University Thesis (1973)

12 T.G.Coleman.Nucl.Inst.and Meth.107 (1973) 399

Chapter Three

13 J.Guy. Private Communication. R.L.

14 G.Fleming. Private Communication. Durham

Chapter Four

15 A.D.Martin, Phys.Lett.65B, 346 (1976)